Tectonics

RESEARCH ARTICLE
10.1029/2017TC004842

Key Points:
- The Qiangtang terrane was situated at 34.6 ± 4.6°N in the Middle Jurassic (reference point: 32.7°N, 89.4°E)
- The Qiangtang terrane did not undergo obvious latitudinal displacement between the Late Triassic and the Middle Jurassic
- The Bangong-Nujiang Ocean reached its maximum width in the Late Triassic and then shrank until it closed by the Cretaceous

Supporting Information:
- Supporting Information S1

Correspondence to:
Z. Sun,
sunzm1209@163.com

Citation:
Cao, Y., Sun, Z., Li, H., Pei, J., Liu, D., Zhang, L., et al. (2019). New paleomagnetic results from Middle Jurassic limestones of the Qiangtang terrane, Tibet: Constraints on the evolution of the Bangong-Nujiang Ocean. *Tectonics*, *38*, 215–232. https://doi.org/10.1029/2017TC004842

Received 9 OCT 2017
Accepted 27 DEC 2018
Accepted article online 3 JAN 2019
Published online 21 JAN 2019

New Paleomagnetic Results From Middle Jurassic Limestones of the Qiangtang Terrane, Tibet: Constraints on the Evolution of the Bangong-Nujiang Ocean

Yong Cao[1], Zhiming Sun[1], Haibing Li[2], Junling Pei[1], Dongliang Liu[2], Lei Zhang[2], Xiaozhou Ye[1], Yong Zheng[2], Xiangli He[2], Chenglong Ge[2], and Wan Jiang[1]

[1]Key Laboratory of Paleomagnetism and Tectonic Reconstruction of Ministry of Natural Resources, Institute of Geomechanics, Chinese Academy of Geological Sciences, Beijing, China, [2]Key Laboratory of Deep-Earth Dynamics of Ministry of Natural Resources, Institute of Geology, Chinese Academy of Geological Sciences, Beijing, China

Abstract To constrain the relationship between the Qiangtang and Lhasa terranes and the evolution of the Bangong-Nujiang Ocean (BNO), we carried out a paleomagnetic investigation of the Middle Jurassic limestone from the Shuanghu region in the southern Qiangtang terrane. Stepwise thermal demagnetization succeeded in isolating high-temperature characteristic directions by either principal component or great circle fitting analyses. The site-mean direction of the 13 sampling sites was $Dg = 334.7°$, $Ig = 51.2°$, $kg = 27.9$, $\alpha_{95} = 8.0°$ (in geographic coordinates) and $Ds = 245.2°$, $Is = 54.1°$, $ks = 113.9$, $\alpha_{95} = 3.9°$ (in stratigraphic coordinates). The paleomagnetic data passed both fold and reversal tests. Both rock magnetic and petrographic investigations suggest a primary magnetization. The paleomagnetic results imply that the paleolatitude of the Qiangtang terrane was 34.6 ± 4.6°N (reference site: 32.7°N, 89.4°E) in the Middle Jurassic. Combined with previous reliable paleomagnetic results, it is suggested that the Qiangtang terrane was situated at a stable paleolatitudinal position and did not undergo obvious N-S displacement between the Late Triassic and the Middle Jurassic. Comparison with the paleomagnetic results available for the Lhasa terrane implies that the width of the BNO was 2,600 ± 710 km (23.4° ± 6.4°) during the Middle Jurassic. The BNO expanded from the Early to Middle Triassic, reached its maximum width in the Late Triassic, and then shrank until it closed by the Cretaceous.

1. Introduction

The uplift and evolution of the Tibetan Plateau (TP), and the underlying controlling processes, are of major interest in geology. The TP is composed of several terranes (Figure 1) and was formed by the collision and combination of these terranes since the early Paleozoic (Metcalfe, 2013; Wang et al., 2014; Xu et al., 2011; Yin & Harrison, 2000; Zhu et al., 2013, 2016). The Qiangtang terrane originated from Gondwana in the Paleozoic (Metcalfe, 2013; Yin & Harrison, 2000) and became attached to the southern edge of the Asian continent in the early Mesozoic (Ding et al., 2013; Mo & Pan, 2006; Peng et al., 2015; Song et al., 2015). The Qiangtang-Lhasa collision commenced following the closure of the Bangong-Nujiang Ocean (BNO), resulting in considerable crustal shortening which has exerted a major influence on the evolution of the TP (Murphy et al., 1997). Hence, the evolution of the BNO and the processes involved in the Qiangtang-Lhasa collision are crucial in understanding the early evolution of the central TP.

Although some research has been undertaken to characterize the evolution of the BNO and the Qiangtang-Lhasa collision, these issues remain under debate. It has been proposed that the BNO opened in the Carboniferous–Permian (Metcalfe, 2013; Pan et al., 2006; Zhu et al., 2013) on the basis of geological evidence or from the Late Permian to the Early Triassic (Fan et al., 2015, 2017) on the basis of geochemical and geochronological evidence. Meanwhile, several studies suggest that the BNO was opened from the Early to Middle Jurassic, as indicated by ophiolites (Wang, Aitchison, et al., 2008; Qu et al., 2010). Furthermore, several researchers have proposed that the BNO acted as a back-arc basin situated between the Lhasa terrane and Qiangtang terrane (Haines et al., 2003; Wang, Aitchison, et al., 2008; Qu et al., 2010). Haines et al. (2003) claimed the Qiangtang and Lhasa terranes are actually a single terrane originating from Gondwana. Based

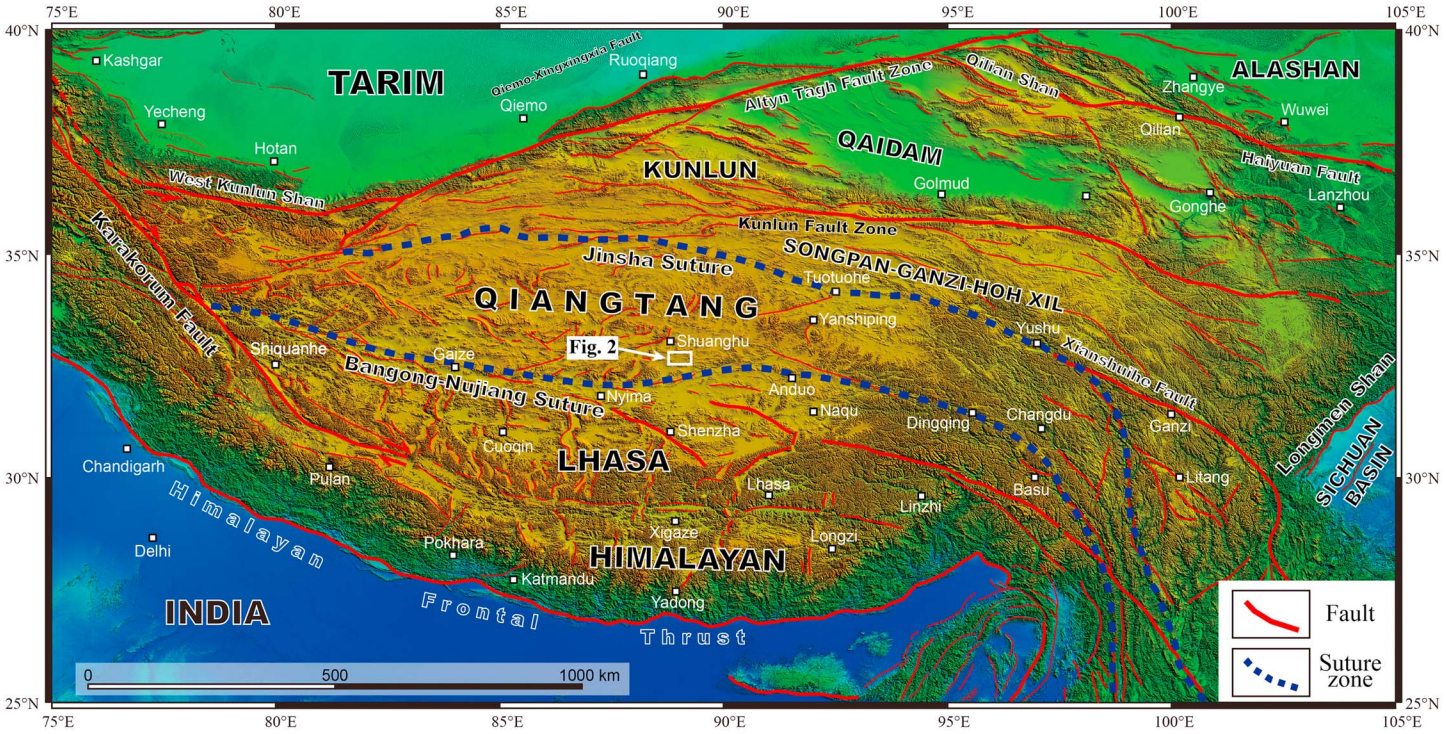

Figure 1. Tectonic sketch map of the Tibetan Plateau and the adjacent region, showing terranes and major faults.

on geochemical analyses of Late Triassic rocks interpreted as remnants of ocean islands, Fan et al. (2017) proposed the BNO was a mature ocean in the Late Triassic. The proposed timing for closure of the BNO (the Qiangtang-Lhasa collision) ranges from the Middle Jurassic to the Late Cretaceous (Baxter et al., 2009; Chen et al., 2017; Kapp et al., 2007; Li et al., 2015; Li et al., 2016; Yan et al., 2016; Zhang et al., 2012; Zhu et al., 2016).

Knowledge of the Mesozoic drift history of the Qiangtang terrane is crucial to understanding the process of the Qiangtang-Lhasa collision and the evolution of the BNO. Paleomagnetism is the only effective method for directly constraining the paleolatitudinal movement of terranes. Previous paleomagnetic results from the Mesozoic rocks in the Qiangtang terrane are important in determining its Mesozoic drift history. However, major uncertainties and limitations remain regarding the existing Middle Jurassic paleomagnetic results. Those from the Yanshiping area reported by Dong et al. (1991) suggested that the Qiangtang terrane was located at 13.0 ± 4.4°N during the Middle Jurassic. However, the paleomagnetic results from 11 sites (102 samples) on the Yanshiping Group limestone indicated a higher paleolatitude of 23.6 ± 7.4°N during the Middle–Late Jurassic (Cheng, Wu, Diao, et al., 2012). Recently, based on two Middle Jurassic paleomagnetic poles from the Yanshiping area, Yan et al. (2016) proposed that the Qiangtang was situated at 23.8 ± 3.9°N and 16.7 ± 2.1°N in the early and late Middle Jurassic, respectively. After elongation/inclination correction (Tauxe & Kent, 2004) of the paleomagnetic results from the Buqu Formation limestone, Ren et al. (2013) suggested that the Qiangtang terrane was located at about 20.4 ± 7.8°N during the Middle Jurassic. However, after comparing the Middle Jurassic inclination recorded in limestone with that in sandstone, Cheng, Wu, Diao, et al. (2012) thought that there was no significant inclination shallowing in the limestone from the Yanshiping area. The extant Middle Jurassic paleomagnetic results from the Qiangtang terrane are all focused on the Yanshiping Group in the north Qiangtang terrane; however, in the case of the paleomagnetic record from the Middle–Late Jurassic Yanshiping Group (clastic and carbonate rocks), the possibility of remagnetization cannot be excluded (Lin & Watts, 1988; Ran et al., 2017). In addition, the carbonate rocks in the orogens may have suffered from remagnetization (Huang, Lippert, Jackson, et al., 2017; Huang, Lippert, Zhang, et al., 2017, and references therein). Hence, additional rock magnetic and petrographic studies should be used to diagnose remagnetization in carbonate rocks (Huang, Lippert, Zhang, et al., 2017).

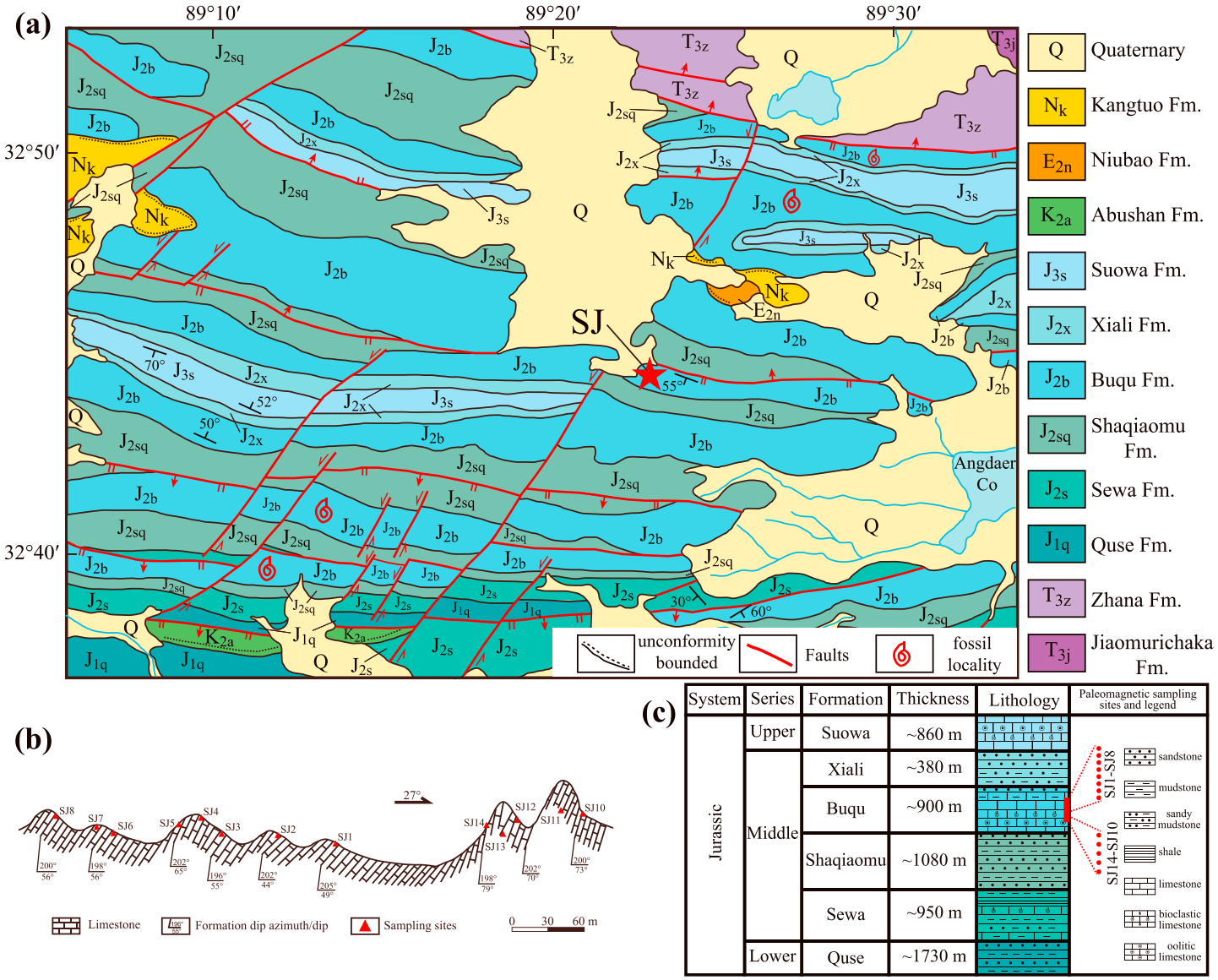

Figure 2. (a) Geological map of the study site (modified from the 1:250,000 scale Angdaer Co regional geological investigation report [I45C004004] by the Jilin Institute of the Geological Survey, 2006). (b) Measured geological section of the Buqu Formation sampling site, showing the locations of the paleomagnetic samples. (c) Simplified Jurassic lithostratigraphic stratigraphy of the study area. The fossil localities of the Buqu Formation in panel (a) are according to Wang, Zhang, et al. (2008).

In this paper, we present the first reliable Middle Jurassic paleomagnetic results for the southern Qiangtang terrane. We have also carried out rock magnetic and petrographic studies to evaluate the reliability of the characteristic remanent magnetization (ChRM) in the studied section. The new Middle Jurassic paleomagnetic results provide reliable constraints on the evolution of the BNO during the Mesozoic.

2. Geological Setting and Sampling

The Qiangtang terrane is situated in the central TP. It is separated from the Songpan-Ganzi-Hoh Xil terrane by the Jinsha suture zone to the north and from the Lhasa terrane by the Bangong-Nujiang suture zone (BNSZ) to the south (Figure 1; Li et al., 2015; Wang et al., 2014; Yin & Harrison, 2000; Zhu et al., 2016). The Longmu Co-Shuanghu suture divides the Qiangtang terrane into the northern Qiangtang terrane and the southern Qiangtang terrane (Li, 1987; Li et al., 2009; Peng et al., 2015; Zhu et al., 2013).

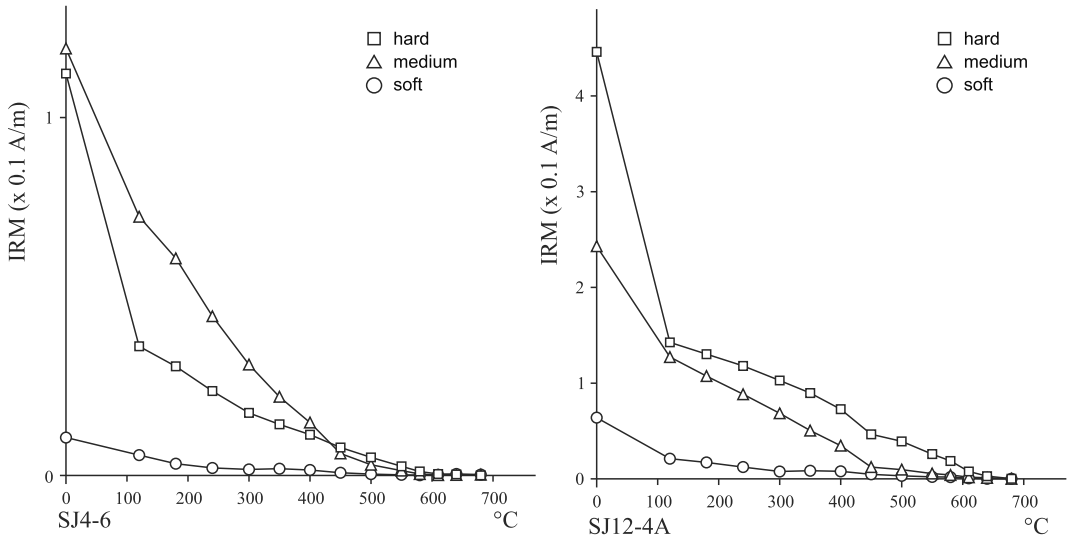

Figure 3. Results of thermal demagnetization of a three-component isothermal remanent magnetization (IRM).

The study area lies on the southern edge of the Qiangtang terrane, about 70 km to the southeast of Shuanghu County. The sampled section is located at 32.7°N, 89.4°E (Figure 2a), about 50 km north of the BNSZ. Samples were collected from the Middle Jurassic Buqu Formation, which consists mainly of gray and gray-black oolitic and bioclastic limestone deposited in a littoral and shallow sea. The Buqu Formation conformably overlies the Shaqiaomu Formation and is overlain by the Xiali Formation. The maximum thickness of the Buqu Formation in the studied area is about 900 m. Fossils identified in the Buqu Formation in the studied area include bivalves (*Protocardia* sp., *Liastrea birmanica*, *Spondylopecten subpunctatus* etc.), ammonoids (*?Choffatia* sp.), and brachiopoda (*Burmirhynchia ovalis Buckman*, *Holcothyris angulate Buckman*), indicative of the Middle Jurassic time (Wang, Zhang, et al., 2008). A total of 13 paleomagnetic sites (approximately 130 samples) were collected for paleomagnetic investigations from the Buqu Formation; samples were collected using a gasoline-powered drill and oriented using a magnetic compass. A simplified cross section of the sampling area is shown in Figure 2b.

3. Laboratory Techniques

Representative samples were subjected to stepwise thermal demagnetization of a three-component isothermal remanent magnetization (IRM; Lowrie, 1990) in the Key Laboratory of Paleomagnetism and Tectonic Reconstruction, Ministry of Natural Resources, China. Stepwise thermal demagnetization of a three-component IRM was conducted using a JR-6 spinner magnetometer. Fields of 2.2, 0.4, and 0.12 T were used to characterize the hard, medium, and soft components, respectively.

Hysteresis loops and first-order reversal curve (FORC) were measured using a Princeton alternating gradient force magnetometer (Model 3900 AGM, nominal sensitivity: 5×10^{-10} Am^2), with 1-T maximum applied field, in the Paleomagnetism and Geochronology Laboratory, Institute of Geology and Geophysics, Chinese Academy of Sciences. Saturation remanence (Mrs), saturation magnetization (Ms), and coercivity (Hc) were obtained after subtracting the paramagnetic contribution.

Every sample was submitted to stepwise thermal demagnetization up to 580 °C performed with an ASC TD-48 thermal demagnetizer with an internal residual field of <10 nT. The thermal demagnetization temperature intervals were usually large (40–60 °C) in the low-temperature range and smaller (20–30 °C) at higher temperatures. Remanent magnetizations were measured with a 2G-755R cryogenic magnetometer in a shielded room with residual fields of <300 nT at the Key Laboratory of Paleomagnetism and Tectonic Reconstruction, Ministry of Natural Resources, China. Principal component analysis (Kirschvink, 1980) or remagnetization circles analysis (Halls, 1978) was carried out to determine the magnetization directions. The average paleomagnetic direction was calculated with Fisher statistics (Fisher, 1953) or the mixed

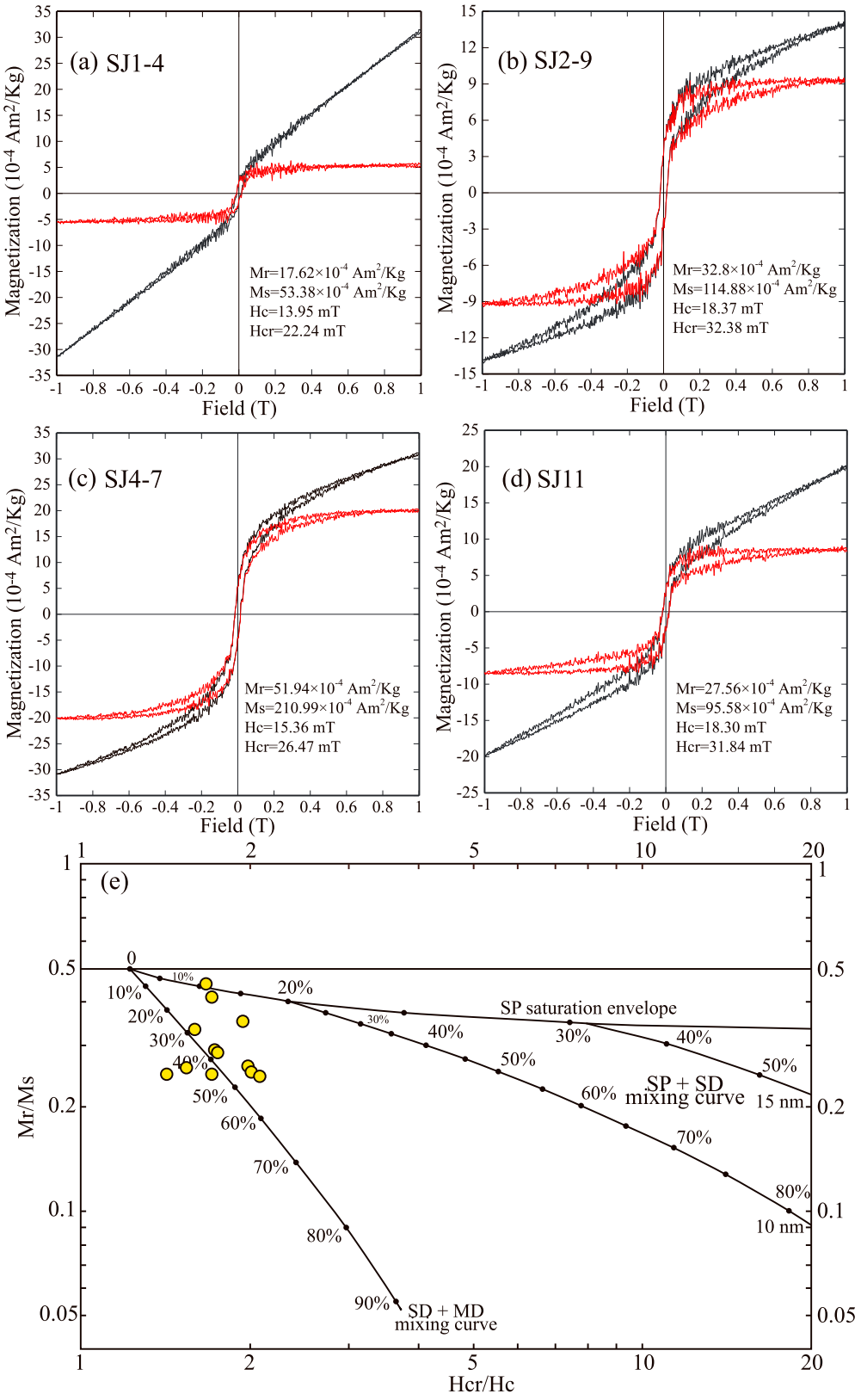

Figure 4. (a–d) Hysteresis loops before (black) and after (red) para-diamagnetic correction of representative samples and (e) Day plot of the hysteresis parameters from the Middle Jurassic Buqu Formation limestone. SD = single domain; MD = multidomain; SP = superparamagnetic domain.

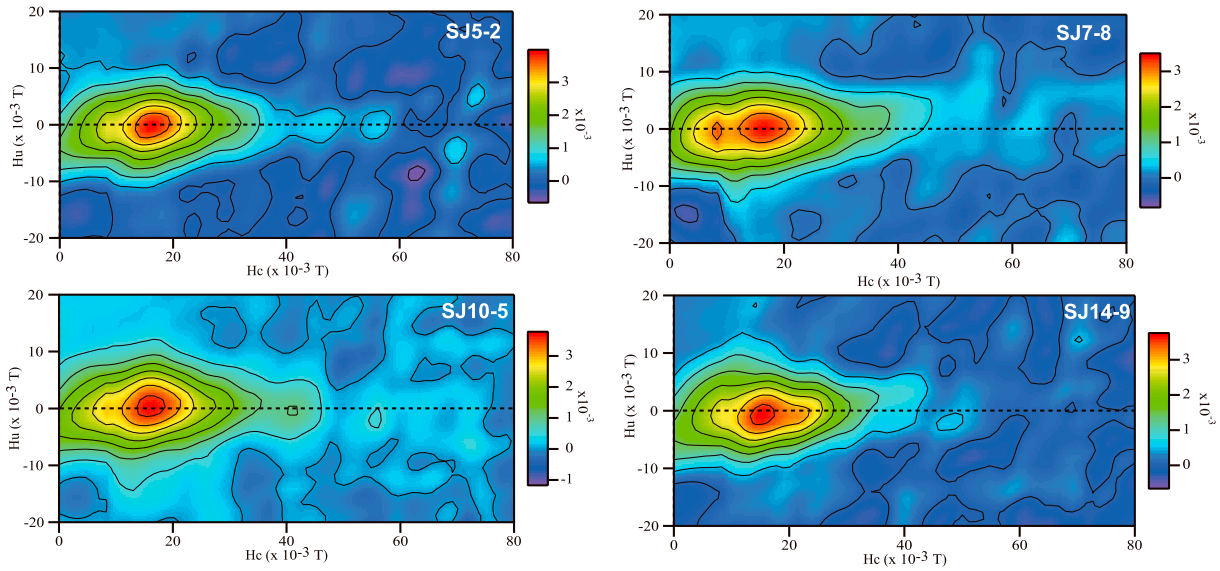

Figure 5. First-order reversal curve diagrams of representative samples from the Middle Jurassic Buqu Formation limestone.

mean of unit vectors and remagnetization great circles (McFadden & McElhinny, 1988). The computer programs *kirsch.exe* developed by Enkin (1990) and *Paleomac* developed by Cogné (2003) were used to analyze the paleomagnetic data.

Scanning electron microscope (SEM) observations with energy-dispersive X-ray spectrometry (EDS) analysis were performed on carbon-coated epoxy resin-embedded polished thin sections of representative samples using a LEO Stereoscan 440 SEM at the Key Laboratory of Deep-Earth Dynamics, Ministry of Land Natural Resources, Institute of Geology, Chinese Academy of Geological Sciences (CAGS).

4. Results

4.1. Rock Magnetic Results

The results of stepwise thermal demagnetization of a three-component IRM for representative samples are shown in Figure 3. The hard component of sample SJ4-6 and the soft, medium, and hard components of sample SJ12-4A exhibited an unblocking temperature of 120 °C, indicative of goethite. The hard and medium components of the sample SJ12-4A show a rapid decrease of magnetization at ~450 °C, which may be indicative of fine-grained magnetite (Dunlop & Özdemir, 2000). Moreover, the hard and medium components of the two representative samples exhibited an unblocking temperature of 580 °C, which may indicate magnetite.

The results of hysteresis loop measurements are shown in Figures 4a–4d. The hysteresis loops obtained after para-diamagnetic correction show that the samples were saturated at about 200 mT. The Hcr and Hc are 17.26–32.8 and 9.74–18.37 mT, respectively (Table S3). These results indicate low-coercivity magnetic minerals that are predominant in the studied section. Furthermore, hysteresis loops are wasp-waisted in shape (Figures 4b–4d), which indicates the coexistence of low-coercivity and high-coercivity magnetic minerals in the studied rocks (Roberts et al., 1995). On the Day plot, hysteresis data for most samples lie near the single-domain (SD) + multidomain (MD) mixing curve (Figure 4e; Day et al., 1977; Dunlop, 2002). The FORC diagrams (Figure 5) exhibit the Hc value of ~15–20 mT at the peak of the distribution. Moreover, the FORC diagrams are consistent with the distribution of vortex state particles, which means the transitional state between the SD and the MD (Roberts et al., 2017). Both Day plot and FORC indicate the SD + MD for the magnetic carrier mineral in the studied section. The domain status of magnetic minerals of limestones in this section is consistent with those of un-remagnetized limestones (Huang, Lippert, Jackson, et al., 2017; Huang, Lippert, Zhang, et al., 2017; Jackson & Swanson-Hysell, 2012; Roberts et al.,

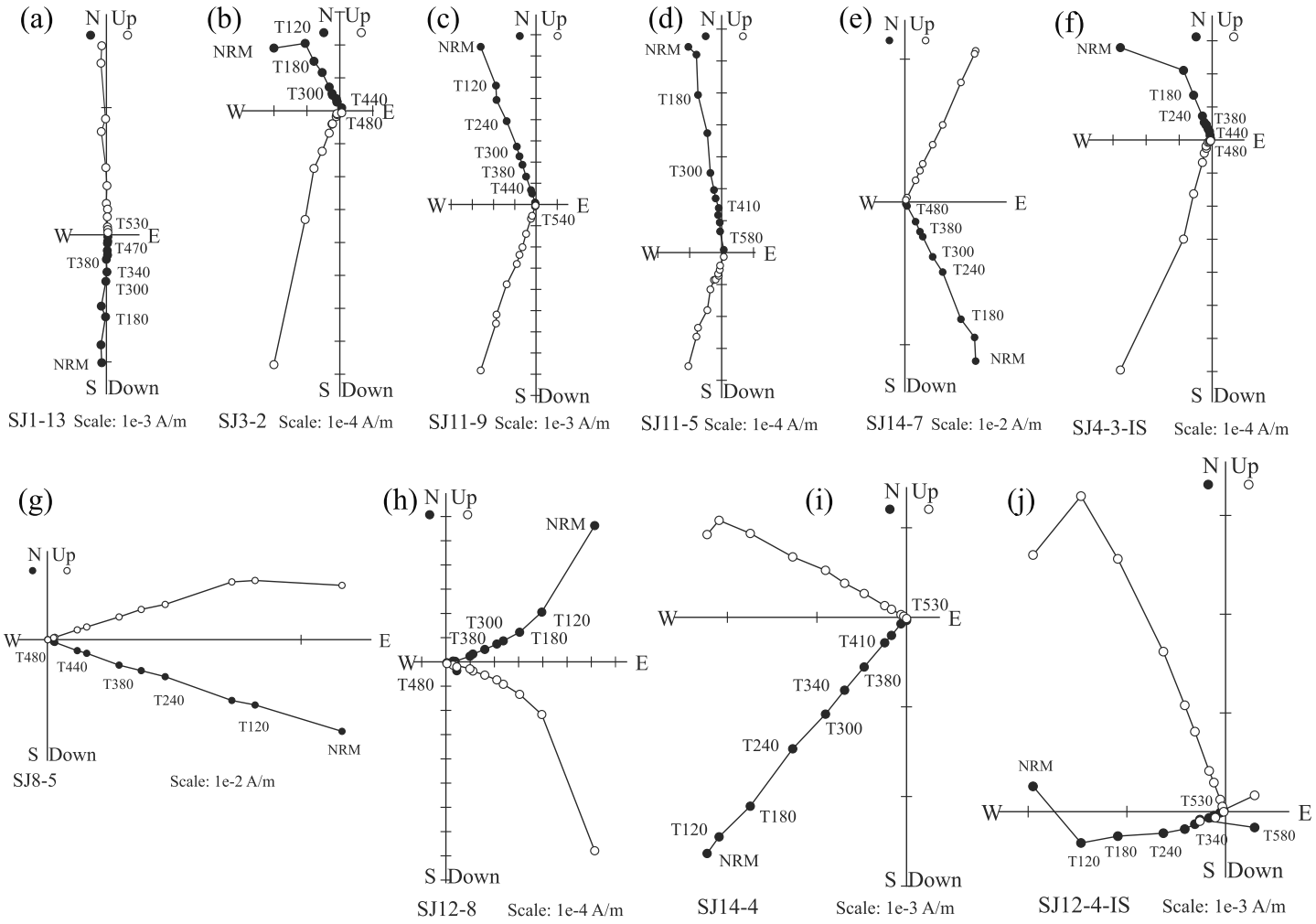

Figure 6. Orthogonal vector diagrams of representative samples determined by principal component analysis (sample number and corresponding site are indicated). Directions were plotted in geographic coordinates. Demagnetization steps are in °C. NRM is the natural remanent magnetization. Open (closed) dots represent vertical (horizontal) projections.

2013). These rock magnetic results suggest, when combined with the thermal demagnetization behavior observed, that magnetite and goethite are the dominant magnetic carriers in the limestone samples.

4.2. Paleomagnetic Results

Representative Zijderveld plots for the samples from the Buqu Formation are shown in Figures 6 and 7. The plots indicate that a randomly oriented viscous low-temperature component was isolated between the NRM and 120 °C for most of the samples (Figures 6b, 6f–6j, and 7a–7d). Other samples exhibited a single higher-temperature component (HTC; Figures 6a and 6c–6e), the direction of which was isolated between 180 and 480 or 580 °C. The HTC often decays toward the origin, and the magnetization directions could be analyzed using principal component analysis (Kirschvink, 1980; Figure 6). In addition, the HTC of some of the samples was distributed along a great circle. The magnetization directions could be analyzed by remagnetization circles analysis (Halls, 1978; Figures 7a–7d), and corresponding site mean of the paleomagnetic directions was calculated using the mixed mean of the principal component and remagnetization great circles (McFadden & McElhinny, 1988), as implemented in the Cogné (2003) software (Figure 7e).

Site-mean directions of the ChRM of the Buqu Formation (Figure 8 and Table 1) are different, both in situ and after bedding correction, from the direction of the present geomagnetic field and the geocentric axial dipole direction at the study locality. The mean direction for the 13 sites is Dg = 334.7°, Ig = 51.2°,

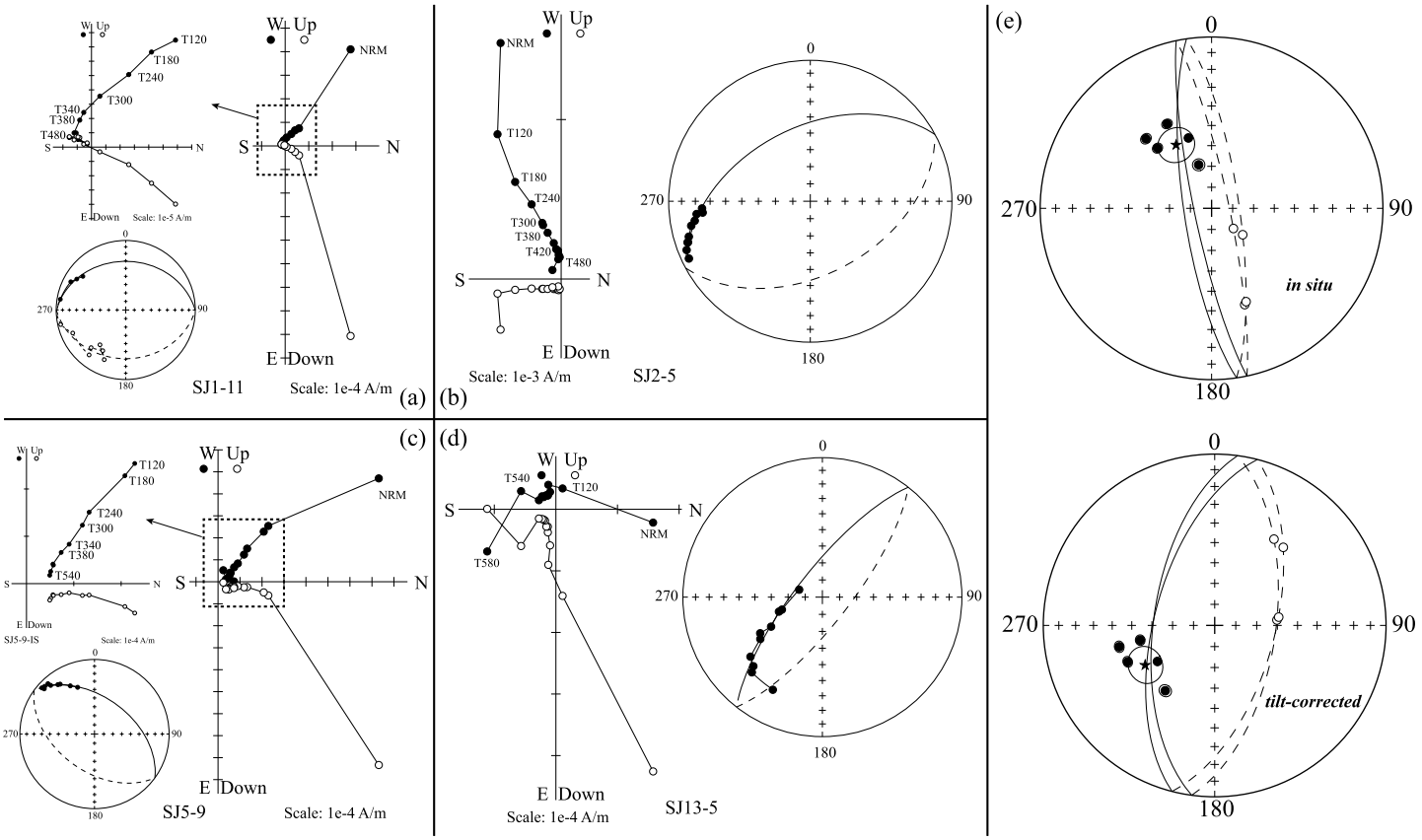

Figure 7. (a–d) Orthogonal vector and equal-area plots of representative samples based on great circles analysis, and (e) equal-area stereographic projection of the site (SJ6) showing the mixed mean of the principal components analysis and the great circles analysis. NRM = natural remanent magnetization.

kg = 27.9, α_{95} = 8.0° (in geographic coordinates) and Ds = 245.2°, Is = 54.1°, ks = 113.9, α_{95} = 3.9° (in stratigraphic coordinates). The corresponding paleopole, computed from the bedding-corrected direction, lies at 1.0°N, 41.1°E, with dp/dm = 3.8°/5.5°.

The tilt-corrected Fisher precision parameter (k) increases significantly from 27.9 to 113.9, with $F(2 * (n2 - 1), 2 * (n1–1)) = 1.98$ at the 95% confidence level and 2.66 at the 99% confidence level. Hence, the site-mean directions passed the McElhinny (1964) fold test. In addition, the site-mean directions passed the McFadden (1990) fold tests at the 95% and 99% confidence levels (in-situ Xi2 = 8.164; tilt-corrected Xi2 = 0.7502; critical "Xi" = 4.2 at 95% confidence, critical "Xi" = 5.86 at 99% confidence). A progressive unfolding correction for the HTC directions shows that k has its maximum value (k = 113.96) at 101% unfolding by the Watson and Enkin (1993) method (Figure 8c). The folding may be attributed to the collision of the Qiangtang terrane and Lhasa terrane during the Late Jurassic–Cretaceous time (Kapp et al., 2007; Song et al., 2015). Furthermore, the site-mean directions passed the reversal test, with a B classification at the 95% confidence level (r = 3.1° < rc = 8.0°; McFadden & McElhinny, 1990).

4.3. SEM Observations

SEM observations of polished thin sections indicate that the morphologies of magnetic minerals in the limestone samples of the Buqu Formation are subeuhedral to euhedral (Figures 9a and 9b), acicular aggregates (Figure 9c), and framboid clusters (Figure 9d). The magnetic minerals are irregular in shape, and their boundaries with the groundmass (mainly calcite) are very clear. This suggests that the magnetic minerals were not influenced by chemical alteration triggered by fluids, hydrothermal, or weathering during orogenic processes.

The EDS results indicate that the samples do not contain sulfides in this study (Figures 9e–9h). It means that the samples in the studied section does not contain pyrite. Rims were not observed around magnetic

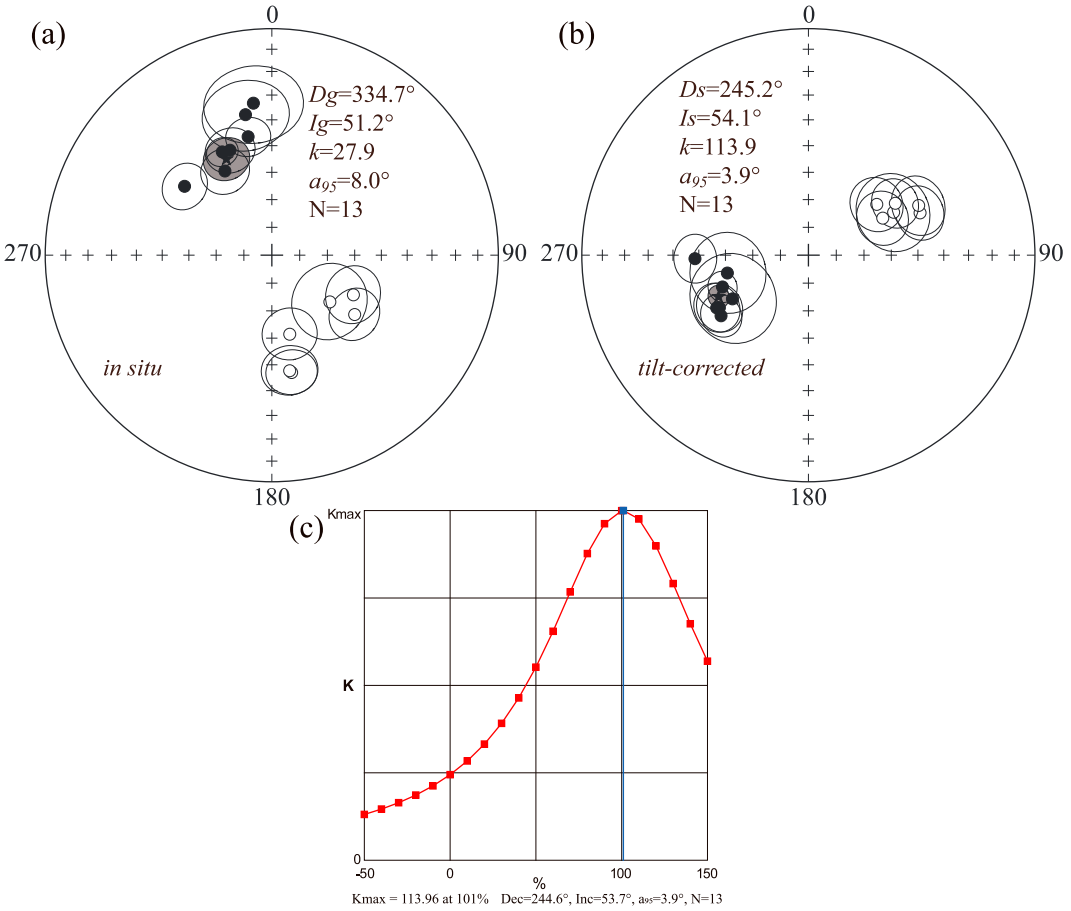

Figure 8. Equal-area projections of site-mean directions from the Middle Jurassic Buqu Formation limestone in the Qiangtang terrane and the progressive unfolding analysis of the higher-temperature component directions using the Watson and Enkin (1993) method. Solid/open symbols represent downward/upward inclinations, the rhombus represents the present geomagnetic field direction, and stars show the overall mean directions at the 13 sites.

minerals according to SEM observations (Figures 9a–9d). This characteristic is different from the results of the authigenic magnetite, which formed as an oxidation product of pyrite or other iron sulfides in the limestone from the TP reported by Huang, Lippert, Zhang, et al. (2017).

The crystal sizes of the magnetic minerals in this study ranged from a few to tens of micrometers. The large magnetite grains may carry a stable remanence (Ma et al., 2018; Yang et al., 2013). The rock magnetic results and EDS analysis (Figures 9e–9h) revealed that the magnetic minerals are mainly composed of magnetite and goethite. The magnetic minerals with acicular aggregates and framboid clusters may imply the presence of secondary goethite in the limestones. However, the ChRM was obtained at temperatures higher than 120 °C in this study, the unblocking temperature of goethite. Furthermore, magnetite coexisting with Fe-oxyhydroxides may represent initial detrital iron phases (Ma et al., 2018). These findings imply that magnetite may have a detrital origin (Abrajevitch & Kodama, 2009; Ma et al., 2018). Based on the above evidence, magnetite is interpreted as of detrital origin and the magnetic carrier of primary remanence in the studied section. Of course, more SEM work is needed to confirm this in the future.

5. Discussion

5.1. Drift History of the Qiangtang Terrane During the Triassic to Jurassic

In this study, we obtained Middle Jurassic paleomagnetic results for the southern Qiangtang terrane. The tilt-corrected paleomagnetic direction was Ds/Is = 245.2°/54.1° with α_{95} = 3.9°, implying that the Qiangtang terrane was situated at 34.6 ± 4.6°N during the Middle Jurassic (reference site: 32.7°N/89.4°E).

Table 1
Site-Mean Paleomagnetic Directions of the High-Temperature Components From the Middle Jurassic Sediments in the Southern Qiangtang Terrane

Site	Strike/ dip (°)	n/N	Dg (°)	Ig (°)	Ds (°)	Is (°)	k	α_{95} (°)
SJ1	115/56	6/10	167.2	−60.7	53.2	−59.1	18.4	9.6
SJ2	112/44	10/10	308.3	49.4	268.4	48.5	16.8	8.2
SJ3	106/55	10/10	334.4	48.1	249.9	56.8	80.0	5.4
SJ4	107/64	7/9	338.3	48.7	239.6	52.4	51.5	8.5
SJ5	112/65	9/9	125.6	−52.9	69.1	−46.2	10.8	9.2
SJ6	108/56	7/10	330.9	55.0	240.3	51.5	30.2	8.5
SJ7	108/55	6/8	128.8	−63.1	63.1	−55.3	7.4	13.6
SJ8	110/56	8/11	115.9	−57.1	65.6	−45.6	10.5	10.1
SJ10	110/73	10/10	348.7	45.7	235.4	51.3	25.4	7.5
SJ11	111/66	6/8	349.4	37.0	257.8	60.0	16.7	14.1
SJ12	112/70	5/9	170.4	−46.4	59.0	−53.1	37.4	8.6
SJ13	111/62	8/10	171.2	−47.2	63.3	−59.9	18.8	9.5
SJ14	108/79	6/9	353.1	32.9	240.3	58.3	13.4	15.8
Mean		13(98)	334.7	51.2			27.9	8.0
					245.2	54.1	113.9	3.9

Corresponding pole: 1.0°N/41.1°E, dp/dm = 3.8°/5.5°
Corresponding paleolatitude: 34.6°N
Reference point: 32.7°N/89.4°E`

Note. Strike:dip direction of beds = 90°; Dip = the mean dip azimuth of site beds; *n*/*N* = number of samples used to calculate mean and measured; *Dg*, *Ig*, *Ds*, *Is* = declination and inclination in geographic and stratigraphic coordinates, respectively; *k* = the best estimate of the precision parameter; α_{95} = the radius that the mean direction lies within 95% confidence.

Several Middle Jurassic paleomagnetic results from the Yanshiping area in the Qiangtang terrane have been reported (Table 2). Results reported by Dong et al. (1990, 1991) and Ren et al. (2013) indicate that the Qiangtang terrane was located at a paleolatitude of 13–24°N during the Middle Jurassic. Moreover, Ren et al. (2013) suggested that the paleomagnetic inclination may have been affected by inclination shallowing in sediments during the depositional and lithification processes. Cheng, Wu, Diao, et al. (2012) presented two sets of paleomagnetic results from the Middle–Late Jurassic Yanshiping Group in the Yanshiping area; however, these data yielded inconsistent results, with respective paleolatitudes of 15.4 ± 7.4°N (sandstone) and 23.6 ± 5.8°N (limestone). Based on a large number of sites, and positive fold and reversal tests, Yan et al. (2016) suggested paleolatitudes of 23.8 ± 5.0°N and 16.7 ± 2.8°N in the Yanshiping area for the Qiangtang terrane during the early and late Middle Jurassic, respectively. Moreover, it is notable that a difference also exists in declination for the previous paleomagnetic results of the Yanshiping Group in the Yanshiping area. Recently, Ran et al. (2017) suggested that the magnetization of the Yanshiping Group from the Yanshiping area is not a primary Jurassic magnetization. Their research results indicate the ChRM directions of the Middle–Upper Jurassic marine rocks are secondary and were possibly affected by fluids in the folding process. Furthermore, the carbonate rocks may have experienced widespread remagnetization that may be difficult to recognize, even with rigorous field tests (Huang, Lippert, Jackson, et al., 2017; Huang, Lippert, Zhang, et al., 2017). In addition, $^{87}Sr/^{86}Sr$ values for the Middle–Upper Jurassic carbonates indicate that these Jurassic marine rocks may have been affected by orogenic-type fluids in the Yanshiping section (Tan et al., 2004), where fluid traces could be clearly recognized from the veins (quartz and calcite) that are commonly present in the Yanshiping region (Ran et al., 2017). Overall, previous Middle Jurassic paleomagnetic studies are all coming from the Yanshiping area in the northern Qiangtang terrane (Table 2). Unfortunately, the review of previous work demonstrates that the existing Jurassic paleomagnetic results from the Yanshiping region are inconsistent and controversial. The published paleomagnetic data sets may have been affected by sedimentary inclination shallowing and/or with remagnetization due to orogenic-type fluids. Hence, the published paleomagnetic results are excluded from the subsequent discussion. More paleomagnetic and petrographic studies are needed to resolve inconsistencies in the Jurassic paleomagnetic data in the Yanshiping region. In this study, the first Middle Jurassic paleomagnetic result was obtained for the southern Qiangtang terrane. The result passed both the fold test and the reversal test. Rock magnetism indicates that magnetite is the major magnetic mineral carrier in the studied section. Both hysteresis parameters and FORC plot in the SD + MD region, which can be regarded as carrying primary remanence and is consistent with those of un-remagnetized limestones (Huang, Lippert, Jackson, et al., 2017; Huang, Lippert, Zhang, et al., 2017; Jackson & Swanson-Hysell, 2012; Roberts et al., 2013). Furthermore, SEM observations indicate that magnetite with an essentially original texture has not been influenced by chemical alteration triggered by fluids, hydrothermal activity, or weathering. Hence, the paleomagnetic direction obtained in this study can be considered as the primary magnetization acquired during the Middle Jurassic period and suitable for tectonic reconstruction of the Qiangtang terrane.

Paleomagnetic data from the Late Triassic sediments in the Qiangtang terrane yielded a paleolatitude of 27.7 ± 4.0°N for the reference site (Song et al., 2012; Table 2). Song et al. (2015) performed a paleomagnetic study of Late Triassic volcanic rocks in the Tuouohe area, which yielded a paleolatitude of 31.1 ± 6.6°N for the reference point (Table 2). Since the paleomagnetic results reported by Song et al. (2015) were obtained from volcanic rocks with accurate zircon U-Pb geochronological constraint (204–213 Ma), and with a sufficient number of samples and positive tests, their Late Triassic paleomagnetic results can be employed to constrain the Late Triassic paleolatitude of the Qiangtang terrane. A Middle Triassic paleomagnetic result with an accurate age (ca. 242–240 Ma) and positive fold test, reported by Song et al. (2017), could be suitable for constraining the paleolatitude of the Qiangtang terrane and indicates a location in 21.0 ± 4.1°N during the

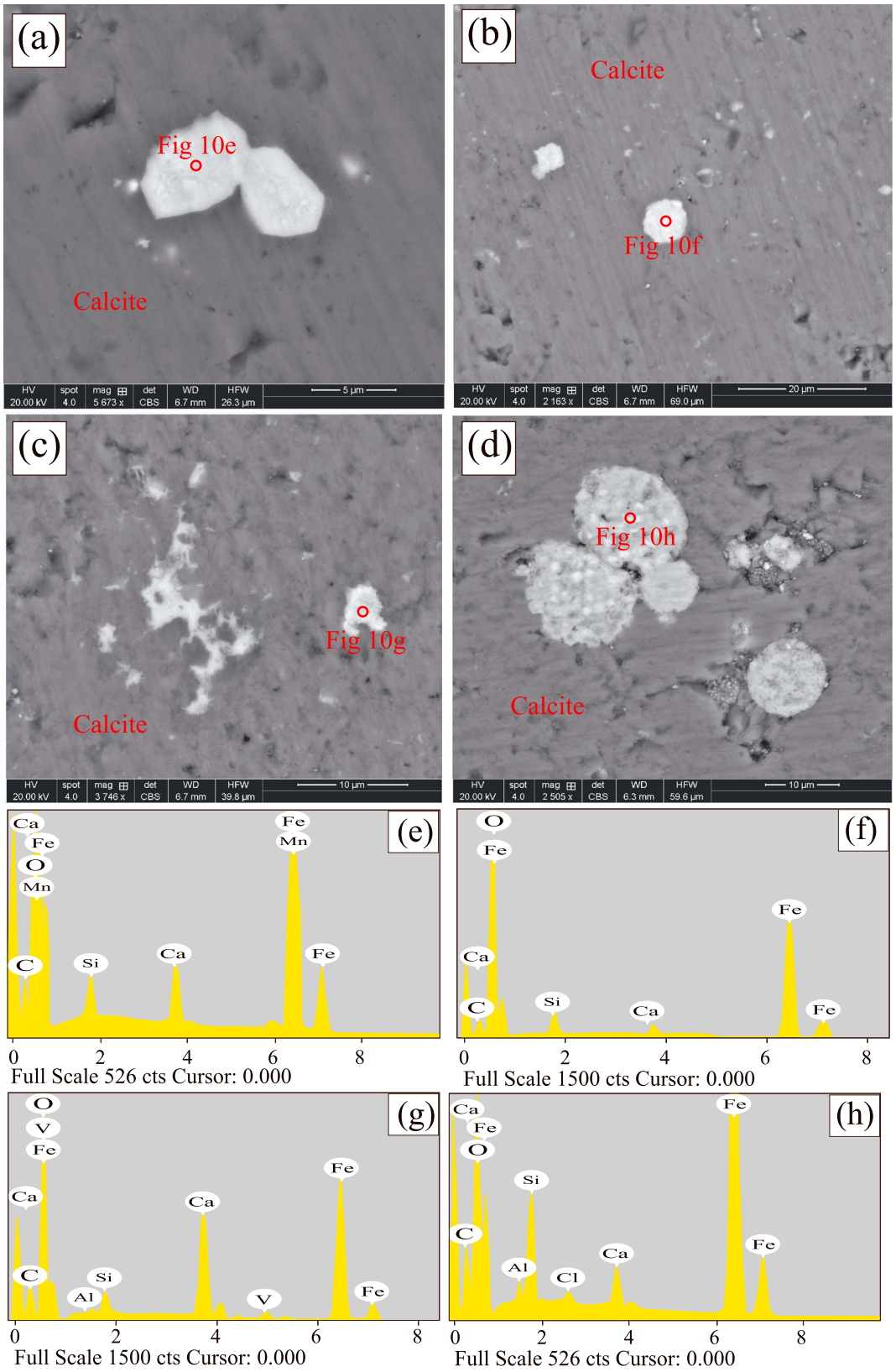

Figure 9. (a–d) Scanning electron microscope backscattered electron images for representative samples and (e–h) the results of energy-dispersive X-ray spectrometry analysis.

Table 2
Triassic and Jurassic Paleomagnetic Poles From the Qiangtang and Lhasa Terranes

Area	Slat. (°N)	Slon. (°E)	Age (Ma)	Rock type	$N(n)$	Plat. (°N)	Plon. (°E).	A_{95} (dp/dm)	Paleolat.	Criteria (Q)	Reference
Qiangtang terrane											
Yanshiping	33.6	92.4	J_3	Mudstone	1(25)	76.9	301.1	7.9/13.2	21.3 ± 10.2	1Ƴ3Ƴ5Ƴ7(4)	Yan et al. (2016)
Yanshiping	33.6	92.1	J_3	Sandstone	20(191)	72.4	318.6	3.9/6.7	20.4 ± 4.9	123F5R7(7)	Yan et al. (2016)
Yanshiping	33.6	92.0	$J_{2\text{-}3}$	Limestone	11(102)	80.0	295.2	7.4/4.5	23.6 ± 5.8	123F5Ƴ7(6)	Cheng, Wu, Diao, et al. (2012)
Yanshiping	33.3	91.6	$J_{2\text{-}3}$	Sandstone	3(8)	77.3	237.2	16.6/27.5	21.7 ± 21.3	1Ƴ3Ƴ5Ƴ7(4)	Dong et al. (1990)
Yanshiping	33.6	92.1	$J_{2\text{-}3}$	Sandstone	24(244)	66.1	332.1	2.7/4.6	19.7 ± 3.5	123F5RƳ(6)	Yan et al. (2016)
Yanshiping	33.6	92.4	J_2	Limestone	27(245)	68.9	313.8	2.1/3.7	16.7 ± 2.8	123Ƴ5RƳ(5)	Yan et al. (2016)
Yanshiping	33.6	92.4	J_2	Sandstone	25(182)	79.1	306.9	3.9/6.3	23.8 ± 5.0	123Ƴ5RƳ(5)	Yan et al. (2016)
Yanshiping	33.6	92.0	J_2	Sandstone	10(68)	71.6	262.0	9.8/5.4	14.4 ± 7.3	123F5R7(7)	Cheng, Wu, Diao, et al. (2012)
Yanshiping	33.4	92.1	J_2	Sandstone	−(15)	60.6	331.1	4.7/8.5	16.0 ± 6.3	1Ƴ3Ƴ5ƳƳ(3)	Dong et al. (1991)
Yanshiping	34.0	92.0	J_2	Sandstone	−(21)	53.6	335.5	3.2/6.0	13.4 ± 4.4	1Ƴ3Ƴ5Ƴ7(4)	Dong et al. (1991)
Yanshiping	33.7	92.1	J_2	Sandstone	20(106)	65.5	327.3	18.3	17.8 ± 18.3	123Ƴ5ƳƳ(4)	Ren et al. (2013)
Yanshiping	33.7	92.1	J_2	Limestone	30(171)	65.6	335.0	7.8	20.4 ± 7.8	123Ƴ5ƳƳ(4)	Ren et al. (2013)
Angdaerco	32.7	89.4	J_2	Limestone	13(98)	1.0	41.1	3.8/5.5	34.6 ± 4.6	123F5R7(7)	This study
Tuotuohe	34.1	92.4	204–213	Volcanic rocks	29(240)	64.0	174.7	6.6	31.1 ± 6.6	123F5R7(7)	Song et al. (2015)
Woruoshan	33.7	87.8	T_3	Sandstone	10(90)	59.2	179.2	4.0	27.7 ± 4.0	123Ƴ5R7(6)	Song et al. (2012)
Xiaochaka	33.1	87.6	T_3	Sandstone	11(105)	65.1	184.4	3.6	27.3 ± 3.6	123Ƴ5R7(6)	Song et al. (2012)
Tuoba	31.3	97.5	T_3	Sandstone	−(20)	31.0	279.5	15.0/32.0	−25.6 ± 21.9	1Ƴ3Ƴ5Ƴ7(4)	Zhu (1985)
Qitadaban	35.7	79.5	T_3	Sandstone	−(6)	−26.5	51.2	8.4/13.9	−20.5 ± 10.8	1Ƴ3Ƴ5Ƴ7(4)	Li et al. (1995)
Yaxico	34.2	93.3	T_3	Volcanic rocks	5(34)	59.0	184.0	13.8/21.2	25.4 ± 17.1	123Ƴ5Ƴ7(4)	Lin and Watts (1988)
Yanshiping	33.5	92.0	242–240	Volcanic rocks	27(−)	63.4	198.8	4.1	21.0 ± 4.1	123F5Ƴ7(6)	Song et al. (2017)
Kongkashan	34.4	79.0	T_2	Sandstone	−(3)	16.9	135.9	5.1/9.2	−15.3 ± 6.8	1Ƴ3Ƴ5Ƴ7(4)	Li et al. (1995)
Rejuechaka	33.7	86.7	T_1	Limestone	2(15)	16.9	202.5	4.9/9.2	−9.1 ± 6.7	1Ƴ3Ƴ5Ƴ7(4)	Cheng, Wu, Guo, et al. (2012)
Lhasa terrane											
Gaize	32.0	84.0	J_3	Sandstone	—	−36.2	106.2	6.9/12.0	−19.3 ± 9.1	1Ƴ3Ƴ5Ƴ7(4)	Yie and Li (1987)
Lhasa	29.6	90.0	J_3	Limestone	−(21)	59.0	280.4	16.6	2.2 ± 16.6	1Ƴ3Ƴ5Ƴ7(4)	Zhu et al. (1981)
Sangxiong	31.1	91.5	J_3	Sandstone	6(32)	50.2	290.1	4.0/7.8	−5.1 ± 5.6	123Ƴ5Ƴ7(5)	Dong et al., (1991)
sssDazi	29.4	91.3	J_{2-3}	Sandstone	4(13)	51.0	293.1	5.3/10.4	−3.7 ± 7.4	1Ƴ3Ƴ5Ƴ7(4)	Dong et al. (1991)
Basu	30.1	96.9	J_2	Sandstone	8(53)	66.8	294.1	7.4/14.5	11.3 ± 10.4	123F5R7(7)	Otofuji et al. (2007)
Sangri	29.3	92.0	~180	Volcanic rocks	60(−)	51.7	305.8	3.5	0.2 ± 3.5	123Ƴ5R7(6)	Li et al. (2016)
Daxiong	30.5	85.0	J	Volcanic rocks	—	28.8	308.8	7.7/13.7	−18.0 ± 10.3	1Ƴ3Ƴ5Ƴ7(4)	Yie and Li (1987)
Cuoqin	30.9	84.7	T_3	Limestone	6(37)	19.6	211.8	10.7	−14.1 ± 10.7	123F5Ƴ7(6)	Zhou et al. (2016)
Dazi	29.4	91.3	T_3	Volcanic rocks	5(22)	8.2	211.6	4.0/7.0	−21.5 ± 5.3	1Ƴ3Ƴ5Ƴ7(4)	Dong et al. (1991)
Qusang	30.0	90.8	T_3	Sandstone	—	30.0	285.0	15.5/32.0	−25.6 ± 22.3	1Ƴ3Ƴ5Ƴ7(4)	Yie and Li (1987)
Deqing	29.6	90.0	T_2	Limestone	—	25.4	295.9	9.6/20.0	−26.7 ± 13.9	1Ƴ3Ƴ5Ƴ7(4)	Ye and Li (1987)
Cuoqin	30.9	84.7	$T_{1\text{-}2}$	Limestone	8(47)	18.9	208.4	3.9	−12.2 ± 3.9	123F5RƳ(6)	Zhou et al. (2016)

Note. Slat. and Slon. = latitude and longitude of the study location, respectively. $N(n)$ = number of sites (samples) used to calculate Fisher mean. Plat. and Plon. = latitude and longitude of the pole, respectively. A_{95} = the radius that the mean pole lies within 95% confidence; dp/dm = semi-axes of elliptical error of the pole at a probability of 95%. Paleolat. = paleolatitude calculated for the reference point at 32.7°N, 89.4°E. Criteria (Q) = data quality criteria (number of criteria met) after Van der Voo (1990): 1 = well determined rock age; 2 = sufficient number of samples, $N \geq 24$, k (or K) ≥ 10, and α_{95} (A_{95}) ≤ 16.0; 3 = systematic stepwise demagnetization; 4 = field tests: F means positive fold test; 5 = structural control and tectonic coherence with the craton or terrane discussed; 6 = presence of reversal: R means positive reversal test and D means dual-polarity characteristic remanent magnetization direction; 7 = no resemblance to paleopole of younger age (by more than a period); "Ƴ" in the criterion column fails to fulfill this criterion.

Middle Triassic (Song et al., 2017). At present, no reliable Early Triassic paleomagnetic data have been reported from the Qiangtang terrane, so the Late Paleozoic paleomagnetic result of Cheng, Wu, Guo, et al. (2012) was used to constrain the Early Triassic paleolatitude of the Qiangtang terrane. We fully acknowledge that more high-quality Triassic paleomagnetic data for the Qiangtang terrane are necessary.

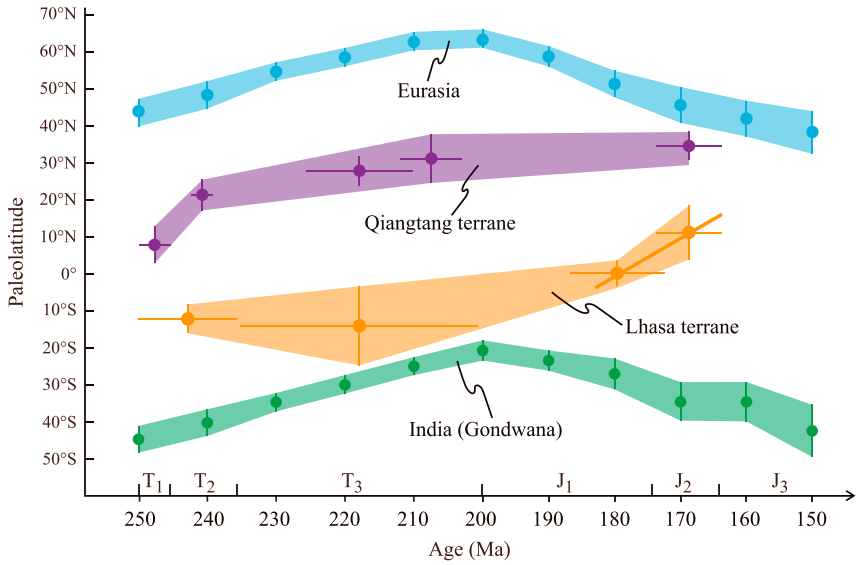

Figure 10. Paleolatitude versus time plot for Qiangtang, Lhasa, Eurasia, and Gondwana (India) during the Mesozoic (reference point: 32.7°N/89.4°E). See Table 2 for values and references. The paleolatitude gaps between Qiangtang and Lhasa terranes during the Late Triassic and the Middle Jurassic is 45.1° ± 9.2° and 23.4° ± 6.4°, respectively. Eurasian and Gondwana (India) paleolatitudes are from Torsvik et al. (2012).

Based on the above analysis, we can constrain the paleolatitudinal variation of the Qiangtang terrane between the Early Triassic and the Middle Jurassic. These results suggest that the Qiangtang terrane was situated at a stable paleolatitudinal position and did not undergo significant latitudinal displacement (3.6° ± 5.6°) from the Late Triassic to the Middle Jurassic (Figure 10). In contrast, the Qiangtang terrane was located further south (~22°) in the Late Paleozoic–Early Triassic than in the Late Triassic to Middle Jurassic. Hence, the Qiangtang terrane may have moved north with a relatively rapid velocity after the Early Triassic and collided with the Songpan-Ganzi terrane in the Late Triassic (Figure 10).

5.2. Evolution of the BNO During the Mesozoic

Knowledge of the paleolatitudinal changes of the Qiangtang terrane and Lhasa terrane in the Mesozoic may contribute to an improved understanding of the evolution of the BNO. The drift history of the Qiangtang terrane from the Triassic to the Middle Jurassic was discussed in section 5.1, and the paleolatitude of the Lhasa terrane was recently reviewed by Li et al. (2016). Their research suggested that the Lhasa terrane drifted north from Gondwana in the Late Triassic with a mean latitudinal plate velocity of ~5 cm/year. According to the kinematic relationships between the Qiangtang and Lhasa terranes, we propose a tentative paleogeographic reconstruction for the central TP in a global setting to infer the evolution of the BNO during the Early–Middle Triassic to the Middle Jurassic (Figure 11). The Triassic and Jurassic paleomagnetic results of the Qiangtang terrane and Lhasa terrane are listed in Table 2. The reference paleopoles used for the paleogeographic positions of Laurasia, Gondwana, the North China Block, and the South China Block are listed in Table S2.

A significant clockwise vertical-axis rotation (127.2° ± 8.8°) relative to stable Eurasia occurred in the studied area since the Middle Jurassic. Our result implies that a significant clockwise rotation extended into central TP. On a more regional scale, clockwise vertical-axis rotations have been widespread within the Qiangtang and Lhasa terranes since the Cretaceous (Cao, Sun, Li, et al., 2017; Cao, Sun, Liu, et al., 2017; Chen et al., 2017; Ma et al., 2017; Meng et al., 2017; Sun et al., 2012; Yang et al., 2015; Yi et al., 2015). Different magnitudes of post-Cretaceous tectonic rotations have been inferred from paleomagnetic results from the west and east of the Qiangtang terrane (Chen et al., 2017). This indicates that the Qiangtang terrane has not behaved completely rigidly over long distances since the Cretaceous, owing to various strike-slip fault systems within the Qiangtang terrane, such that heterogeneous deformation has probably occurred within it.

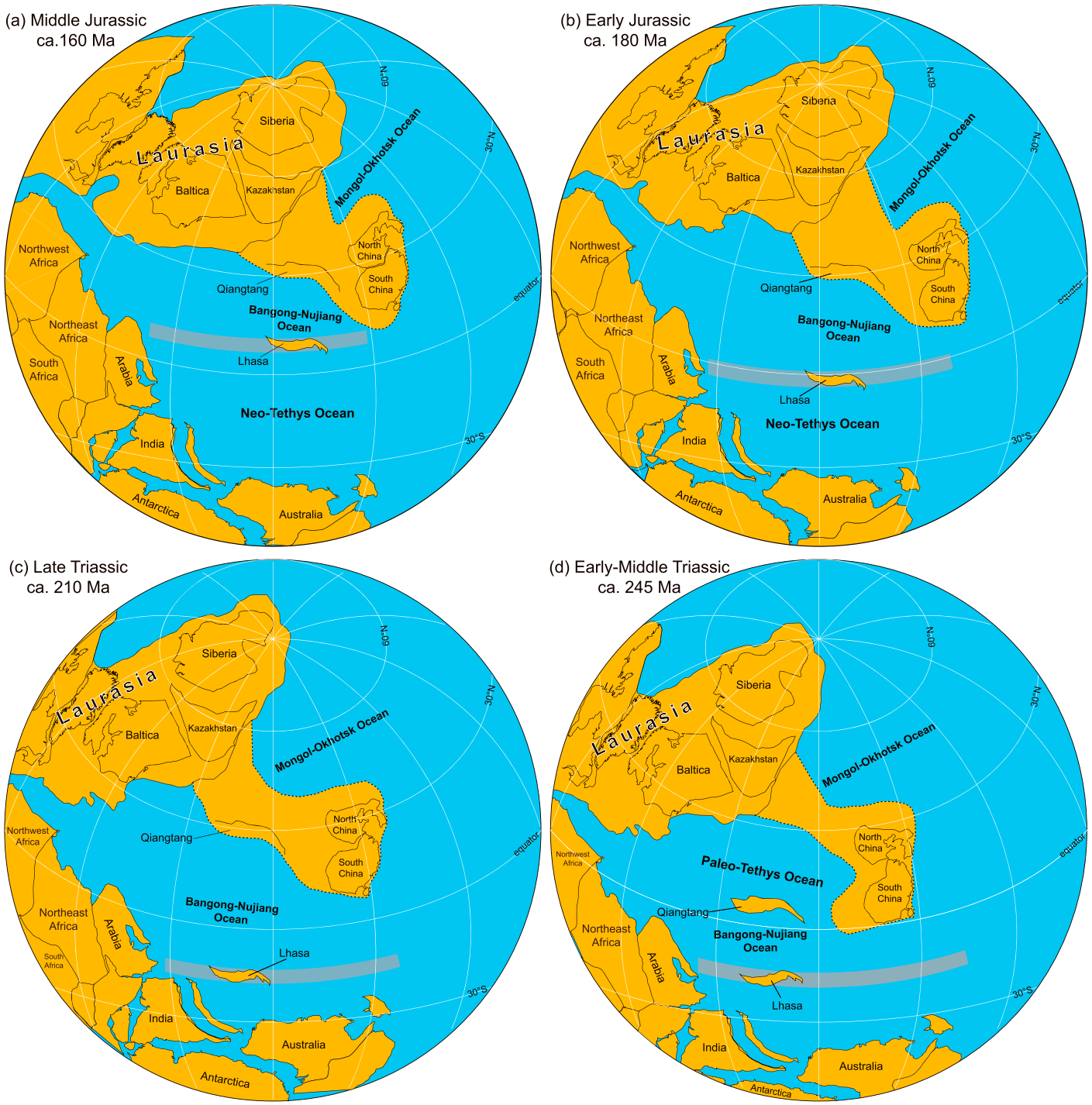

Figure 11. Schematic maps showing the evolution of the Bangong-Nujiang Ocean during the Triassic to the Middle Jurassic. There is no limitation on the relative longitudes of the blocks. The reference paleopoles used for the geographic positions of Laurasia, Gondwana, the North China Block, and the South China Block are listed in Table S2.

According to the paleontological evidence, the Triassic coral fauna in the Qiangtang terrane are similar to those of the Songpan-Ganzi terrane (Bo, Wang, et al., 2017; Bo, Yao, et al., 2017). This indicates that the Qiangtang terrane was close to the Songpan-Ganzi terrane during the Triassic, which resulted in the migration and exchange of the benthonic organisms (Bo, Yao, et al., 2017). Hence, the paleolongitude of the

Qiangtang terrane may be consistent with that of the Songpan-Ganzi terrane, which became separated from the South China Block by the Longmenshan fault zone to the east.

The Qiangtang terrane moved rapidly northward during the Early to Late Triassic (Figure 10) and accreted to the southern edge of the Asian continent in the Late Triassic (Song et al., 2015). The Lhasa terrane did not undergo obvious latitudinal displacement during the Triassic. Hence, the width of the BNO expanded from the Early Triassic to the Late Triassic. The distance between the Qiangtang and Lhasa terranes was 5,000 ± 1,020 km (45.1° ± 9.2° in latitude) during the Late Triassic (Figure 10). Thus, the Qiangtang and Lhasa terranes cannot have been a single terrane in the Mesozoic, contrary to the proposal of Haines et al. (2003). There should have been a fully developed paleo-ocean between the Qiangtang and Lhasa terranes. The Qiangtang terrane maintained a relatively stable paleolatitudinal position during the Late Triassic to the Middle Jurassic. The Lhasa terrane was rifted away from Gondwana and moved to the north after the Late Triassic (Li et al., 2016) and reached a paleolatitude of 11.3 ± 10.4°N during the Middle Jurassic (reference point: 32.7°N, 89.4°E; Otofuji et al., 2007).

Some researchers have suggested that the closure of the BNO and collision of the Qiangtang and Lhasa terranes occurred in the Middle Jurassic. For example, based on the low-grade metamorphism at the northern edge of the Lhasa terrane, Xu et al. (1985) proposed that the collision of the Qiangtang and Lhasa terranes occurred in the Middle Jurassic. In addition, according to the analysis of ductile shear deformation and syntectonic geochronology of the basement in the Anduo-Nierong area, Shi et al. (2017) also considered that the collision between the Qiangtang and Lhasa terranes occurred in the Middle Jurassic. However, geological studies have implied that the metamorphism of the Ando-Nirong area may represent the accretion of microcontinents within the BNO and the Qiangtang terrane (Guynn et al., 2013; Zhu et al., 2016). The Middle Jurassic stratigraphy in the south Qiangtang terrane mainly comprises littoral and neritic facies and widespread limestones (Wang & Fu, 2018). This indicates that the paleo-ocean on the south of the Qiangtang terrane was not closed during the Middle Jurassic. On the other hand, geochemical and geochronological studies of ophiolites and magmatic rocks along the BNSZ imply that the BNO did not close in the Middle Jurassic (Fan et al., 2015; Li et al., 2015; Wang et al., 2016; Zhang et al., 2012). In addition, based on the analysis of multidisciplinary evidence from the BNSZ and its adjacent regions, Zhu et al. (2016) considered that the BNO had closed in the Early Cretaceous. Comparison of the Jurassic paleolatitudinal positions of the Qiangtang and Lhasa terranes indicates that the width of the BNO was 2,600 ± 710 km (23.4° ± 6.4°) during the Middle Jurassic (Figures 10 and 11). Therefore, the closure of the BNO (the collision between the Qiangtang and Lhasa terranes) should have occurred after the Middle Jurassic.

According to the drift history of the Qiangtang and Lhasa terranes (Figures 10 and 11), the evolution of the BNO during the Mesozoic can be summarized as follows. The BNO expanded from the Early Triassic to the Late Triassic and reached its maximum width in the Late Triassic (Figure 11). Subsequently, the BNO shrank since the Lhasa terrane had rifted from Gondwana and moved to the north (Figure 11). Collision between the Qiangtang and Lhasa terranes resulted in the closure of the BNO in the Cretaceous.

6. Conclusions

This study presents new and reliable paleomagnetic results from 13 limestone sites of the Middle Jurassic Buqu Formation in the southern Qiangtang terrane. The mean paleomagnetic direction of 13 sites is $Dg = 154.7°$, $Ig = 51.2°$, $kg = 27.9$, $\alpha_{95} = 8.0°$ (in geographic coordinates) and $Ds = 65.2°$, $Is = -54.1°$, $ks = 113.9$, $\alpha_{95} = 3.9°$ (in stratigraphic coordinates). The paleomagnetic data passed both fold and reversal tests. Rock magnetic and petrographic investigations suggest a primary origin for the isolated remanence direction. The implied paleolatitude suggests that the Qiangtang terrane was situated at 34.6 ± 4.6°N during the Middle Jurassic (reference point: 32.7°N/89.4°E). Comparison of our paleomagnetic result with previous ones for the Qiangtang and Lhasa terranes indicates that (1) the Qiangtang terrane was located at a stable paleolatitudinal position and did not undergo obvious latitudinal displacement (3.6° ± 5.6°) from the Late Triassic to the Middle Jurassic; (2) the width of the BNO in the Middle Jurassic was 2,600 ± 710 km (23.4° ± 6.4°); and (3) the BNO expanded during the Early Triassic to Late Triassic, reaching its maximum width in the Late Triassic, until it shrank and was closed by the Cretaceous.

Acknowledgments
Data to support this study are available in the supporting information. Support for this work was obtained from the National Natural Science Foundation of China (NSFC, grant nos. 41672218 and 91855216), the China Geological Survey (grant no. DD20160022-03), and the Special Funds of Basic Scientific Research Expenses of CAGS (grants nos. JYYWF 201810 and JYYWF20182102). We are extremely grateful to John Geissman (the Editor), Augusto Rapalini (the Associate Editor), Yo-ichiro Otofuji, María Paula Iglesia Llanos, Ross N. Mitchell, and an anonymous reviewer for their constructive comments and suggestions.

References

Abrajevitch, A., & Kodama, K. (2009). Biochemical vs. detrital mechanism of remanence acquisition in marine carbonates: A lesson from the K-T boundary interval. *Earth and Planetary Science Letters*, *286*(1–2), 269–277. https://doi.org/10.1016/j.epsl.2009.06.035

Baxter, A. T., Aitchison, J. C., & Zyabrev, S. V. (2009). Radiolarian age constraints on Mesotethyan ocean evolution, and their implications for development of the Bangong-Nujiang suture, Tibet. *Journal of the Geological Society of London*, *166*(4), 689–694. https://doi.org/10.1144/0016-76492008-128

Bo, J., Wang, X., Gao, J., Yao, J., Wang, G., & Hou, E. (2017). Upper Triassic reef coral fauna in the Renacuo area, northern Tibet, and its implications for palaeobiogeography. *Journal of Asian Earth Sciences*, *146*, 114–133. https://doi.org/10.1016/j.jseaes.2017.05.006

Bo, J., Yao, J., Liao, W., & Deng, Z. (2017). Triassic scleractinian corals in China: A review of present knowledge. *Acta Geologica Sinica*, *91*(1), 270–282. https://doi.org/10.1111/1755-6724.13077

Cao, Y., Sun, Z. M., Li, H. B., Pei, J. L., Jiang, W., Xu, W., Zhao, L. S., et al. (2017). New Late Cretaceous paleomagnetic data from volcanic rocks and red beds from the Lhasa terrane and its implications for the paleolatitude of the southern margin of Asia prior to the collision with India. *Gondwana Research*, *41*, 337–351. https://doi.org/10.1016/j.gr.2015.11.006

Cao, Y., Sun, Z. M., Liu, D. L., Zhang, L., Ye, X. Z., Zheng, Y., & He, X. L. (2017). Late Cretaceous paleomagnetic results in the Nyima area from the northern margin of the Lhasa block and its tectonic implications. *Acta Petrologica Sinica*, *33*(12), 3989–3998. (in Chinese with English abstract)

Chen, W. W., Zhang, S. H., Ding, J. K., Zhang, J. H., Zhao, X. X., Zhu, L. D., et al. (2017). Combined paleomagnetic and geochronological study on Cretaceous strata of the Qiangtang terrane, central Tibet. *Gondwana Research*, *41*, 373–389. https://doi.org/10.1016/j.gr.2015.07.004

Cheng, X., Wu, H. N., Diao, Z. B., Wang, H. J., Zhang, X. D., Ma, L., Zhou, Y. N., et al. (2012). New paleomagnetic results of the Middle-Late Jurassic rocks from northern Qiangtang Block, west China. *Chinese Journal of Geophysics*, *55*, 3399–3409. (in Chinese with English abstract). https://doi.org/10.6038/j.issn.0001-5733.2012.10.023

Cheng, X., Wu, H. N., Guo, Q., Hou, B. N., Xia, L. Y., Wang, H. J., Diao, Z. B., et al. (2012). Paleomagnetic results of late Paleozoic rocks from northern Qiangtang Block in Qinghai-Tibet Plateau, China. *Science China Earth Sciences*, *55*(1), 67–75. https://doi.org/10.1007/s11430-011-4287-x.

Cogné, J. P. (2003). PaleoMac: A Macintosh™ application for treating paleomagnetic data and making plate reconstructions. *Geochemistry, Geophysics, Geosystems*, *4*(1), 1007. https://doi.org/10.1029/2001GC000227.

Day, R., Fuller, M., & Schmidt, V. (1977). Hysteresis properties of titanomagnetites: Grain-size and compositional dependence. *Physics of the Earth and Planetary Interiors*, *13*(4), 260–267. https://doi.org/10.1016/0031-9201(77)90108-X

Ding, L., Yang, D., Cai, F. L., Pullen, A., Kapp, P., Gehrels, G. E., Zhang, L. Y., et al. (2013). Provenance analysis of the Mesozoic Hoh-Xil-Songpan-Ganzi turbidites in northern Tibet: Implications for the tectonic evolution of the eastern Paleo-Tethys Ocean. *Tectonics*, *32*, 34–48. https://doi.org/10.1002/tect.20013

Dong, X. B., Wang, Z. M., Tan, C. Z., Yang, H. X., Cheng, L. R., & Zhou, Y. X. (1990). New paleomagnetic results from Yadong-Golmud geoscience transect and a preliminary study on the model of terranes evolution in Qinghai-Xizang Plateau. *Chinese Academy of Geological Sciences*, *21*, 139–148. (in Chinese with English abstract)

Dong, X. B., Wang, Z. M., Tan, C. Z., Yang, H. X., Cheng, L. R., & Zhou, Y. X. (1991). New results of paleomagnetic studies of the Qinghai-Tibet Plateau. *Geology Reviews*, *37*, 160–164. (in Chinese with English abstract)

Dunlop, D. J. (2002). Theory and application of the Day plot (M_{rs}/M_s versus H_{cr}/H_c): 2. Application to data for rocks, sediments, and soils. *Journal of Geophysical Research*, *107*(B3), 2057. https://doi.org/10.1029/2001JB000487

Dunlop, D. J., & Özdemir, Ö. (2000). Effect of grain size and domain state on thermal demagnetization tails. *Geophysical Research Letters*, *27*(9), 1311–1314. https://doi.org/10.1029/1999GL008461

Enkin, R. J. (1990). Formation et déformation de l'Asie depuis la fin de l'ère primaire: les apports de l'étude paléomagnétique des formations secondaires de Chine du Sud. Ph D thesis, University of de Paris, Paris, 333 pp.

Fan, J. J., Li, C., Wang, M., Liu, Y. M., & Xie, C. M. (2017). Remnants of a Late Triassic ocean island in the Gufeng area, northern Tibet: Implications for the opening and early evolution of the Bangong–Nujiang Tethyan Ocean. *Journal of Asian Earth Sciences*, *135*, 35–50. https://doi.org/10.1016/j.jseaes.2016.12.015

Fan, J. J., Li, C., Xie, C. M., Wang, M., & Chen, J. W. (2015). The evolution of the Bangong–Nujiang Neo-Tethys ocean: Evidence from zircon U–Pb and Lu–Hf isotopic analyses of Early Cretaceous oceanic islands and ophiolites. *Tectonophysics*, *655*, 27–40. https://doi.org/10.1016/j.tecto.2015.04.019

Fisher, R. (1953). Dispersion on a sphere. *Proceedings of the Royal Society of London. Series A*, *217*(1130), 295–305. https://doi.org/10.1098/rspa.1953.0064

Guynn, J., Tropper, P., Kapp, P., & Gehrels, G. E. (2013). Metamorphism of the Amdo metamorphic complex, Tibet: Implications for the Jurassic tectonic evolution of the Bangong suture zone. *Journal of Metamorphic Geology*, *31*(7), 705–727. https://doi.org/10.1111/jmg.12041

Haines, S., Klemperer, S. L., Brown, L., Guo, J., Mechie, J., Meissner, R., et al. (2003). INDEPTH III seismic data: From surface observations to deep crustal processes in Tibet. *Tectonics*, *22*(1), 1001. https://doi.org/10.1029/2001TC001305.

Halls, H. C. (1978). The use of converging remagnetization circles in paleomagnetism. *Physics of the Earth and Planetary Interiors*, *16*(1), 1–11. https://doi.org/10.1016/0031-9201(78)90095-X

Huang, W., Lippert, P. C., Jackson, M. J., Dekkers, M. J., Zhang, Y., Li, J., et al. (2017). Remagnetization of the Paleogene Tibetan Himalayan carbonate rocks in the Gamba area: Implications for reconstructing the lower plate in the India-Asia collision. *Journal of Geophysical Research: Solid Earth*, *122*, 808–825. https://doi.org/10.1002/2016JB013662

Huang, W., Lippert, P. C., Zhang, Y., Jackson, M. J., Dekkers, M. J., Li, J., et al. (2017). Remagnetization of carbonate rocks in southern Tibet: Perspectives from rock magnetic and petrographic investigations. *Journal of Geophysical Research: Solid Earth*, *122*, 2434–2456. https://doi.org/10.1002/2017JB013987

Jackson, M., & Swanson-Hysell, N. L. (2012). Rock magnetism of remagnetized carbonate rocks: Another look. *Geological Society of London, Special Publication*, *371*(1), 229–251. https://doi.org/10.1144/SP371.3

Kapp, P., DeCelles, P. G., Gehrels, G. E., Heizler, M., & Ding, L. (2007). Geological records of the Lhasa-Qiangtang and Indo-Asian collisions in the Nima area of central Tibet. *Geological Society of America Bulletin*, *119*(7-8), 917–933. https://doi.org/10.1130/B26033

Kirschvink, J. L. (1980). The least-squares line and plane and the analysis of palaeomagnetic data. *The Rapid Calculation of Potential Anomalies*, *62*(3), 699–718. https://doi.org/10.1111/j.1365-246X.1980.tb02601.x.

Li, C. (1987). The Longmucuo-Shuanghu-Lancangjiang plate suture and the north boundary of distribution of Gondwana facies Permo-Carboniferous system in northern Xizang, China. *Journal of Changchun College of Geology*, *17*, 155–166. (in Chinese with English abstract)

Li, C., Zhai, G. Y., Wang, L. Q., Yin, F. G., & Mao, X. C. (2009). An important window for understanding the Qinghai-Tibet Plateau—A review on research progress in recent years of Qingtang area, Tibet. China. *Geological Bulletin of China*, *28*, 1169–1177. (in Chinese with English abstract)

Li, Y. A., Li, Q., Zhang, H., Sun, D. J., Cao, Y. D., & Wu, S. Z. (1995). Paleomagnetic study of Tarim and its adjacent area as well as the formation and evolution of Tarim basin. *Xinjiang Geology*, *13*(4), 293–376. (in Chinese with English abstract)

Li, Y. L., Wang, C. S., Dai, J. G., Xu, G. Q., Hou, Y. L., & Li, X. H. (2015). Cretaceous volcanic rocks in south Qiangtang terrane: Products of northward subduction of the Bangong–Nujiang Ocean? *Journal of Asian Earth Sciences*, *104*, 69–83. https://doi.org/10.1016/j.jseaes.2014.09.033

Li, Z. Y., Ding, L., Lippert, P. C., Song, P. P., Yue, Y. H., & van Hinsbergen, D. J. J. (2016). Paleomagnetic constraints on the Mesozoic drift of the Lhasa terrane (Tibet) from Gondwana to Eurasia. *Geology*, *44*(9), 727–730. https://doi.org/10.1130/G38030.1

Lin, J. L., & Watts, D. R. (1988). Palaeomagnetic results from the Tibetan Plateau. *Philosophical Transactions of the Royal Society A*, *327*(1594), 239–262. https://doi.org/10.1098/rsta.1988.0128

Lowrie, W. (1990). Identification of ferromagnetic minerals in a rock by coercivity and unblocking temperature properties. *Geophysical Research Letters*, *17*(2), 159–162. https://doi.org/10.1029/GL017i002p00159

Ma, Y., Yang, T., Bian, W., Jin, J., Wang, Q., Zhang, S., Wu, H., et al. (2018). A stable southern margin of Asia during the Cretaceous: Paleomagnetic constraints on the Lhasa-Qiangtang collision and the maximum width of the Neo-Tethys. *Tectonics*, *37*, 3853–3876. https://doi.org/10.1029/2018TC005143

Ma, Y., Yang, T., Bian, W., Jin, J., Wang, Q., Zhang, S., et al. (2017). Paleomagnetic and geochronologic results of latest Cretaceous lava flows from the Lhasa terrane and their tectonic implications. *Journal of Geophysical Research: Solid Earth*, *122*, 8786–8809. https://doi.org/10.1002/2017JB014743

McElhinny, M. W. (1964). Statistical significance of the fold test in palaeomagnetism. *Geophysical Journal International*, *8*(3), 338–340. https://doi.org/10.1111/j.1365-246X.1964.tb06300.x

McFadden, P. L. (1990). A new fold test for palaeomagnetic studies. *Geophysical Journal International*, *103*(1), 163–169. https://doi.org/10.1111/j.1365-246X.1990.tb01761.x

McFadden, P. L., & McElhinny, M. W. (1988). The combined analysis of remagnetization circles and direct observations in palaeomagnetism. *Earth and Planetary Science Letters*, *87*(1-2), 161–172. https://doi.org/10.1016/0012-821X(88)90072-6

McFadden, P. L., & McElhinny, M. W. (1990). Classification of the reversal test in palaeomagnetism. *Geophysical Journal International*, *103*(3), 725–729. https://doi.org/10.1111/j.1365-246X.1990.tb05683.x

Meng, J., Zhao, X., Wang, C., Liu, H., Li, Y., Han, Z., et al. (2017). Palaeomagnetism and detrital zircon U–Pb geochronology of Cretaceous redbeds from central Tibet and tectonic implications. *Geological Journal*, *53*. https://doi.org/10.1002/gj.3070(5), 2315–2333.

Metcalfe, I. (2013). Gondwana dispersion and Asian accretion: Tectonic and palaeogeographic evolution of eastern Tethys. *Journal of Asian Earth Sciences*, *66*, 1–33. https://doi.org/10.1016/j.jseaes.2012.12.020

Mo, X. X., & Pan, G. T. (2006). From the Tethys to the formation of the Qinghai-Tibet Plateau: Constrained by tectono-magmatic events. *Earth Science Frontiers*, *13*(6), 43–51. (in Chinese with English abstract)

Murphy, M. A., Yi, A., Garrison, T. M., Durr, S. B., Chen, Z., Ryerson, F. J., Kidd, W. S. F., et al. (1997). Did the Indo-Asian collision alone create the Tibetan Plateau? *Geology*, *26*(10), 958–722. https://doi.org/10.1130/0091-7613(1998)026<0958:DTIACA>2.3.CO;2.

Otofuji, Y., Mu, C. L., Tanaka, K., Miura, D., Inokuchi, H., Kamei, R., Tamai, M., et al. (2007). Spatial gap between Lhasa and Qiangtang blocks inferred from Middle Jurassic to Cretaceous paleomagnetic data. *Earth and Planetary Science Letters*, *262*(3-4), 581–593. https://doi.org/10.1016/j.epsl.2007.08.013.

Pan, G. T., Mo, X. X., Hou, Z. Q., Zhu, D. C., Wang, L. Q., Li, G. M., Zhao, Z. D., et al. (2006). Spatial-temporal framework of the Gangdese Orogenic Belt and its evolution. *Acta Petrologica Sinica*, *23*, 521–533. (in Chinese with English abstract)

Peng, T. P., Zhao, G. C., Fan, W. M., Peng, B. X., & Mao, Y. S. (2015). Late Triassic granitic magmatism in the eastern Qiangtang, Eastern Tibetan Plateau: Geochronology, petrogenesis and implications for the tectonic evolution of the Paleo-Tethys. *Gondwana Research*, *27*(4), 1494–1508. https://doi.org/10.1016/j.gr.2014.01.009.

Qu, X. M., Xin, H. B., Zhao, Y. Y., Wang, R. J., & Fan, X. T. (2010). Opening time of Bangong Lake Middle Tethys oceanic basin of the Tibet Plateau: Constraints from petro-geochemistry and zircon U-Pb LAICPMS dating of mafic ophiolites. *Earth Science Frontiers*, *17*, 53–63. (in Chinese with English abstract)

Ran, B., Deng, B., Wang, C., Zhao, X., Li, Y., Zhang, Y., Meng, J., et al. (2017). Kinematics of the crust around the Tanggula Shan in north-central Tibet: Constraints from paleomagnetic data. *Gondwana Research*, *48*, 124–133. https://doi.org/10.1016/j.gr.2017.04.017

Ren, H. D., Yan, M. D., Meng, Q. Q., Song, C. H., & Fang, X. M. (2013). "E/I" corrected paleomagnetic inclination indicates 100 km N-S shortening of the Qiangtang terrane since the Middle Jurassic. *Chinese Journal of Geology*, *48*(2), 543–556. (in Chinese with English abstract)

Roberts, A. P., Almeida, T. P., Church, N. S., Harrison, R. J., Heslop, D., Li, Y., Li, J., et al. (2017). Resolving the origin of pseudo-single domain magnetic behavior. *Journal of Geophysical Research: Solid Earth*, *122*, 9534–9558. https://doi.org/10.1002/2017JB014860

Roberts, A. P., Cui, Y., & Verosub, K. L. (1995). Wasp-waisted hysteresis loops: Mineral magnetic characteristics and discrimination of components in mixed magnetic systems. *Journal of Geophysical Research*, *100*(B9), 17,909–17,924. https://doi.org/10.1029/95JB00672.

Roberts, A. P., Florindo, F., Chang, L., Heslop, D., Jovane, L., & Larrasoaña, J. C. (2013). Magnetic properties of pelagic marine carbonates. *Earth-Science Reviews*, *127*, 111–139. https://doi.org/10.1016/j.earscirev.2013.09.009

Shi, W., Dong, S., Huang, X., Chen, H., & Cui, J. (2017). Jurassic deformation at the western margin of the East Asia continent: A case study of ductile deformation in the central segment of the Bangong Co-Nujiang belt. *Journal of Geomechanics*, *23*(4), 515–525. (in Chinese with English abstract)

Song, C. Y., Wang, J., Fu, X. G., Feng, X. L., Chen, M., & He, L. (2012). Late Triassic paleomagnetic data from the Qiangtang terrane of Tibetan Plateau and their tectonic significances. *Journal of Jilin University(Earth Science Edition)*, *42*(2), 241–250.

Song, P. P., Ding, L., Li, Z. Y., Lippert, P. C., Yang, T. S., Zhao, X. X., Fu, J. J., et al. (2015). Late Triassic paleolatitude of the Qiangtang block: Implications for the closure of the Paleo-Tethys Ocean. *Earth and Planetary Science Letters*, *424*, 69–83. https://doi.org/10.1016/j.epsl.2015.05.020

Song, P. P., Ding, L., Lippert, P. C., & Li, Z. Y. (2017). Late Triassic closure of the Paleo-Tethys Ocean in Central Tibet implied by paleomagnetism of Middle Triassic lavas from the Qiantang block. Abstract [GP51A-0783] presented at 2017 Fall Meeting, AGU, New Orleans, LA, 11–15 Dec.

Sun, Z. M., Pei, J. L., Li, H. B., Xu, W., Jiang, W., Zhu, Z. M., Wang, X. S., et al. (2012). Palaeomagnetism of late cretaceous sediments from southern Tibet: Evidence for the consistent palaeolatitudes of the southern margin of Eurasia prior to the collision with India. *Gondwana Research*, *21*(1), 53–63. https://doi.org/10.1016/j.gr.2011.08.003

Tan, F. W., Wang, J., Wang, X. L., & Du, B. W. (2004). Analysis of carbon and oxygen isotope composition and sedimentary environment of the Yanshiping area of the Qiangtang Basin in Middle-Late Jurassic. *Acta Geoscientia Sinica*, *25*(2), 119–126. (in Chinese with English Abstract)

Tauxe, L., & Kent, D. V. (2004). A simplified statistical model for the geomagnetic field and the detection of shallow bias in paleomagnetic inclinations: Was the ancient magnetic field dipolar? In: Channell, J.E.T., Kent, D.V., Lowrie, W., Meert, J.M. (Eds.), *Timescales of the paleomagnetic field* Geophysical Monograph Series 145. American Geophysical Union, Washington, D. C, pp. 101–115. https://doi.org/10.1029/145GM08

Torsvik, T. H., Van de Voo, R., Preeden, U., Niocaill, C. M., Steinberger, B., Doubrovine, P. V., et al. (2012). Phanerozoic polar wander, palaeogeography and dynamics. *Earth-Science Reviews*, *114*(3-4), 325–368. https://doi.org/10.1016/j.earscirev.2012.06.007

Van der Voo, R. (1990). The reliability of paleomagnetic data. *Tectonophysics*, *184*(1), 1–9. https://doi.org/10.1016/0040-1951(90)90116-P.

Wang, B. D., Wang, L. Q., Chung, S. L., Chen, J. L., Yin, F. G., Liu, H., et al. (2016). Evolution of the Bangong–Nujiang Tethyan ocean: Insights from the geochronology and geochemistry of mafic rocks within ophiolites. *Lithos*, *245*, 18–33. https://doi.org/10.1016/j.lithos.2015.07.016

Wang, C. S., Dai, J. G., Zhao, X. X., Li, Y. L., Graham, S. A., He, D. F., et al. (2014). Outward-growth of the Tibetan Plateau during the Cenozoic: A review. *Tectonophysics*, *621*, 1–43. https://doi.org/10.1016/j.tecto.2014.01.036

Wang, J., & Fu, X. (2018). Sedimentary evolution of the Qiangtang Basin. *Geology in China*, *45*(2), 237–259. (in Chinese with English abstract)

Wang, W. L., Aitchison, J. C., Lo, C. H., & Zeng, Q. G. (2008). Geochemistry and geochronology of the amphibolite blocks in ophiolitic mélanges along Bangong-Nujiang suture, central Tibet. *Journal of Asian Earth Sciences*, *33*(1-2), 122–138. https://doi.org/10.1016/j.jseaes.2007.10.022

Wang, Y. S., Zhang, S. Q., Zheng, C. Z., Li, Q. W., Chen, D. C., Li, X. B., & Yu, W. X. (2008). Biostratigraphic of the Middle Jurassic Sewa, Shaqiaomu and Bu Qu formations in the Quruiqianai area, south Qiangtang basin, northern Tibet, China. *Geological Bulletin of China*, *27*(1), 92–100. (in Chinese with English abstract)

Watson, G. S., & Enkin, R. J. (1993). The fold test in paleomagnetism as a parameter estimation problem. *Geophysical Research Letters*, *20*(19), 2135–2137. https://doi.org/10.1029/93GL01901

Xu, R. H., Schärer, U., & Allègre, C. J. (1985). Magmatism and metamorphism in the Lhasa block (Tibet): A geochronological study. *Journal of Geology*, *93*(1), 41–57. https://doi.org/10.1086/628918

Xu, Z., Yang, J., Li, H., Ji, S., Zhang, Z., & Liu, Y. (2011). On the tectonics of the India-Asia collision. *Acta Geologica Sinica*, *85*(1), 1–33. (in Chinese with English abstract)

Yan, M. D., Zhang, D. W., Fang, X. M., Ren, H. D., Zhang, W. L., Zan, J. B., et al. (2016). Paleomagnetic data bearing on the Mesozoic deformation of the Qiangtang Block: Implications for the evolution of the Paleo- and Meso-Tethys. *Gondwana Research*, *39*, 292–316. https://doi.org/10.1016/j.gr.2016.01.012

Yang, T., Hyodo, M., Zhang, S., Maeda, M., Yang, Z., Wu, H., & Li, H. (2013). New insights into magnetic enhancement mechanism in Chinese paleosols. *Palaeogeography Palaeoclimatology Palaeoecology*, *369*, 493–500. https://doi.org/10.1016/j.palaeo.2012.11.016

Yang, T. S., Ma, Y. M., Zhang, S. H., Bian, W. W., Yang, Z. Y., Wu, H. C., et al. (2015). New insights into the India–Asia collision process from Cretaceous paleomagnetic and geochronologic results in the Lhasa terrane. *Gondwana Research*, *28*(2), 625–641. https://doi.org/10.1016/j.gr.2014.06.010.

Yi, Z. Y., Huang, B. C., Yang, L. K., Tang, X. D., Yan, Y. G., Qiao, Q. Q., et al. (2015). A quasi-linear structure of the southern margin of Eurasia prior to the India–Asia collision: First paleomagnetic constraints from Upper Cretaceous volcanic rocks near the western syntaxis of Tibet. *Tectonics*, *34*, 1431–1451. https://doi.org/10.1002/2014TC003571

Yie, X. H., & Li, J. F. (1987). Palaeomagnetism and evolution of Tibet plates and Tethys. *Journal of Chengdu College of Geology*, *14*, 65–79. (in Chinese with English abstract)

Yin, A., & Harrison, T. M. (2000). Geologic evolution of the Himalayan–Tibetan orogen. *Annual Review of Earth and Planetary Sciences*, *28*(1), 211–280. https://doi.org/10.1146/annurev.earth.28.1.211.

Zhang, K. J., Zhang, Y. X., Tang, X. C., & Xia, B. (2012). Late Mesozoic tectonic evolution and growth of the Tibetan Plateau prior to the Indo-Asian collision. *Earth Science Reviews*, *114*(3-4), 236–249. https://doi.org/10.1016/j.earscirev.2012.06.001.

Zhou, Y. N., Cheng, X., Yu, L., Yang, X. F., Su, H. L., Peng, X. M., et al. (2016). Paleomagnetic study on the Triassic rocks from the Lhasa terrane, Tibet, and its paleogeographic implications. *Journal of Asian Earth Sciences*, *121*, 108–119. https://doi.org/10.1016/j.jseaes.2016.02.006

Zhu, D. C., Li, S. M., Cawood, P. A., Wang, Q., Zhao, Z. D., Liu, S. A., & Wang, L. Q. (2016). Assembly of the Lhasa and Qiangtang terranes in central Tibet by divergent double subduction. *Lithos*, *245*, 7–17. https://doi.org/10.1016/j.lithos.2015.06.023

Zhu, D. C., Zhao, Z. D., Niu, Y. L., Dilek, Y., Hou, Z. Q., & Mo, X. X. (2013). The origin and pre-Cenozoic evolution of the Tibetan Plateau. *Gondwana Research*, *23*(4), 1429–1454. https://doi.org/10.1016/j.gr.2012.02.002.

Zhu, Z. W. (1985). Comparative significance of apparent polar wander path of Xizang and its adjacent regions since Phanerozoic. *Chinese Journal of Geophysics*, *28*, 219–225. (in Chinese)

Zhu, Z. W., Zhu, X. Y., & Zhang, Y. M. (1981). Palaeomagnetic observation in Xizang and continental drift. *Chinese Journal of Geophysics*, *24*(1), 40–49. (in Chinese with English abstract)